An Earth Observation Challenge: 2D+t and 3D+t dynamics of the upper ocean

Satellite measurements of Ocean Surface Current ?

A necessary tool

Essential needs

P. Niiler (2009) Oceanography in 2025

Oceanography of 2025 will require observations and realistic modeling of the circulation patterns that contain the vertical motion of the upper 200 m. Models will be compared not by how well they assimilate or replicate the sea level or reproduce the geostrophic velocity, but rather by how their internal vorticity and thermal energy and fresh water balances maintain ageostrophic velocity structures and the associated vertical circulations. This task calls for development and implementation of continued new methods and instruments for direct velocity observations of the oceans.

Initial Gulf Stream Depiction (circulated by Benjamin Franklin, circa 1770)

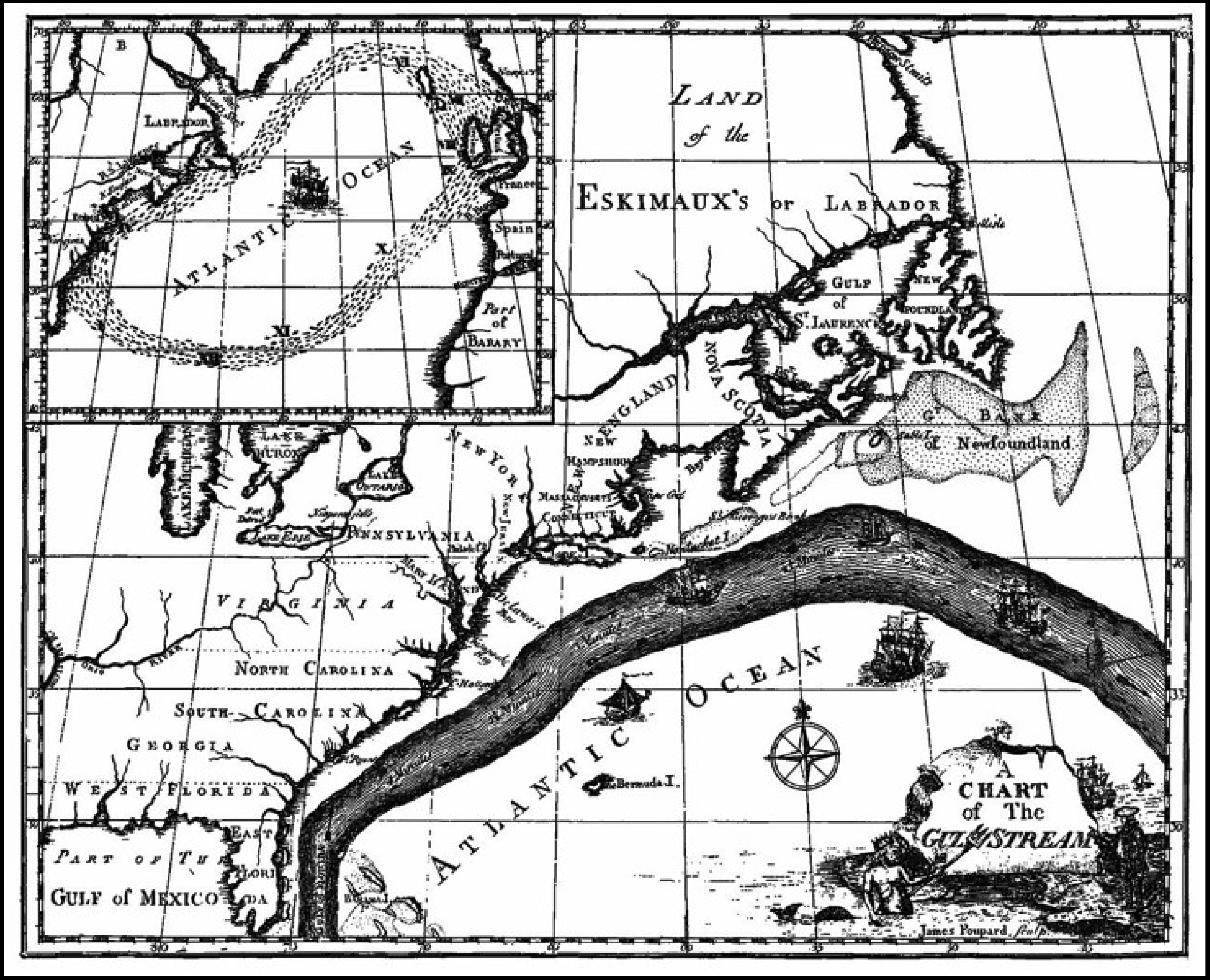

What do we model: A Fully Turbulent Ocean !

All the oceans are crowded with a large number of mesoscale eddies (>100 km). This vision has been confirmed by modelling studies (OFES, POP - 2003) with a 1/10th degree resolution performed on the ES

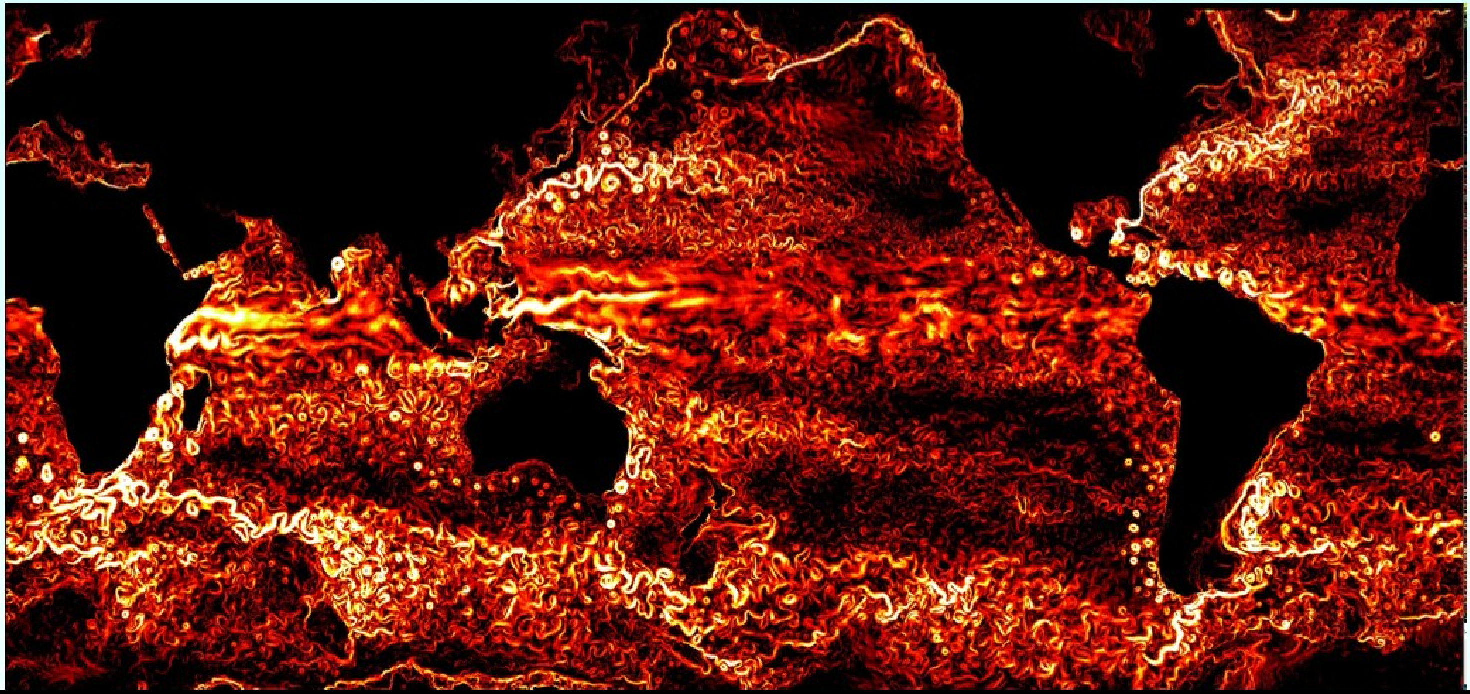

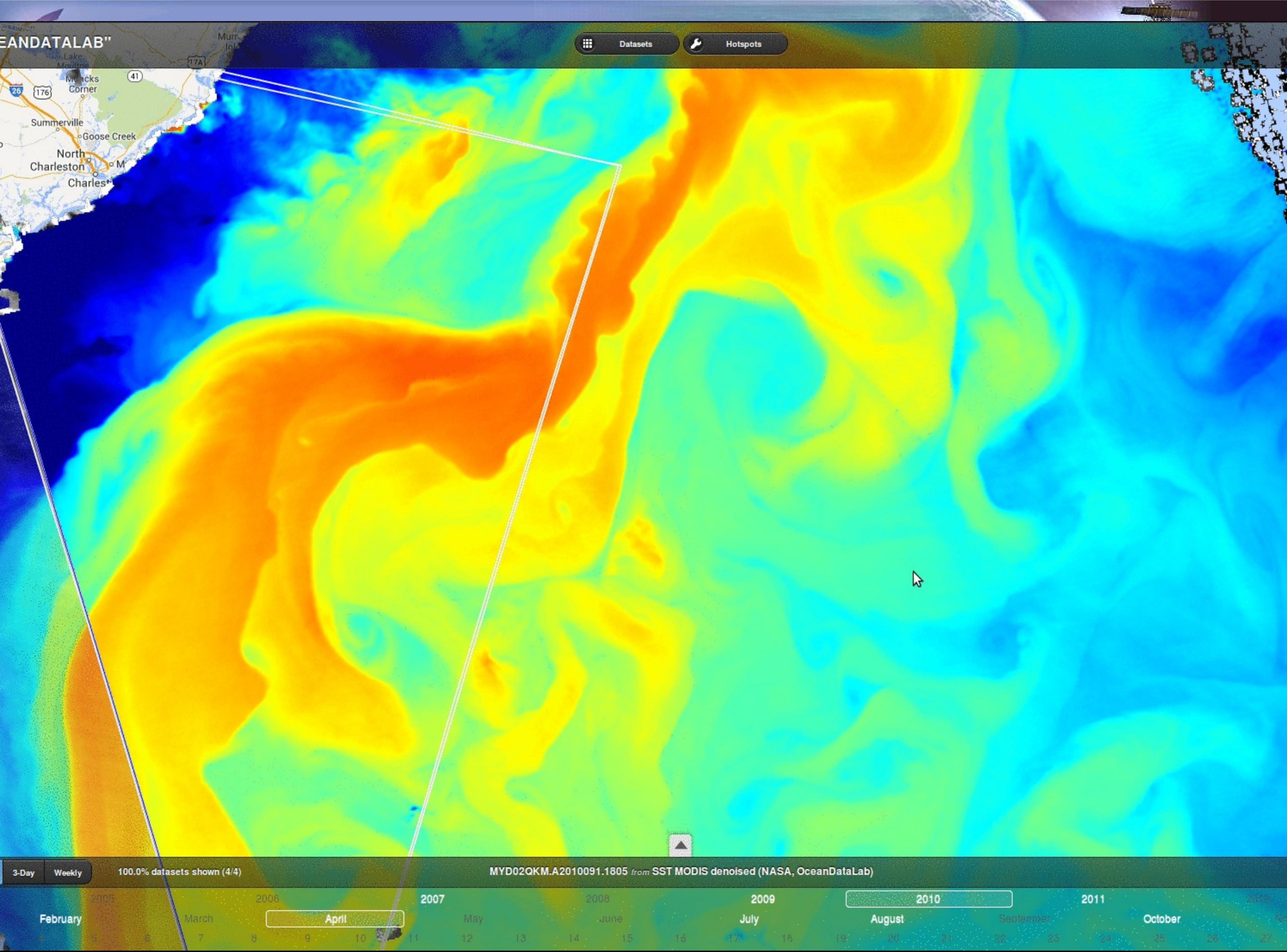
EANDATALAB"
Datasets
Hotspots
Summerville
Goose Creek
North Charleston
3-Day
Weekly
100.0% datasets shown (4/4)
MYD02QKM.A2010091.1805 from SST MODIS denoised (NASA, OceanDataLab)
2007
2009
2010
2011
February
April
July
August
October

Meso- and submeso-scale details: the DrFab principle ?

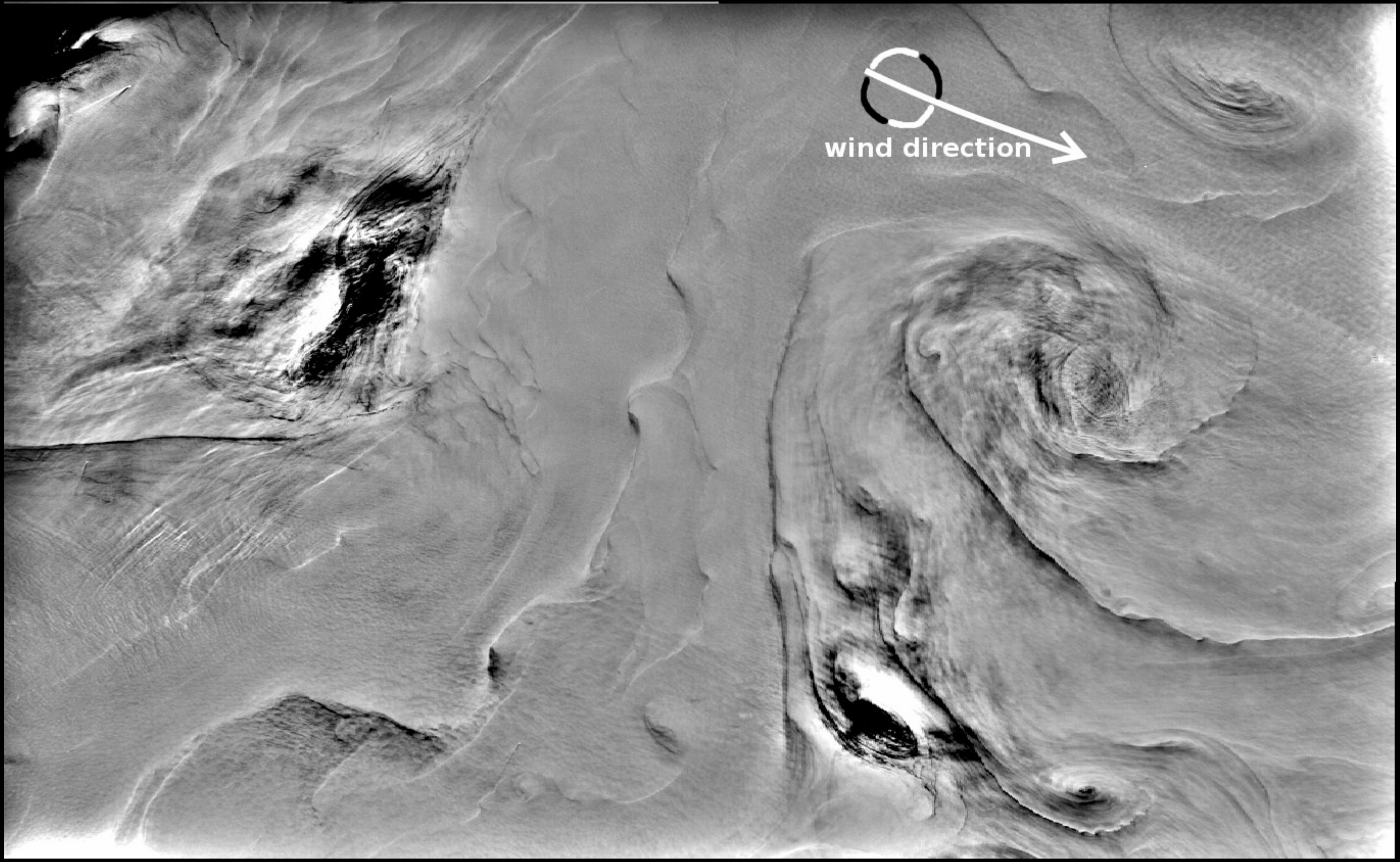

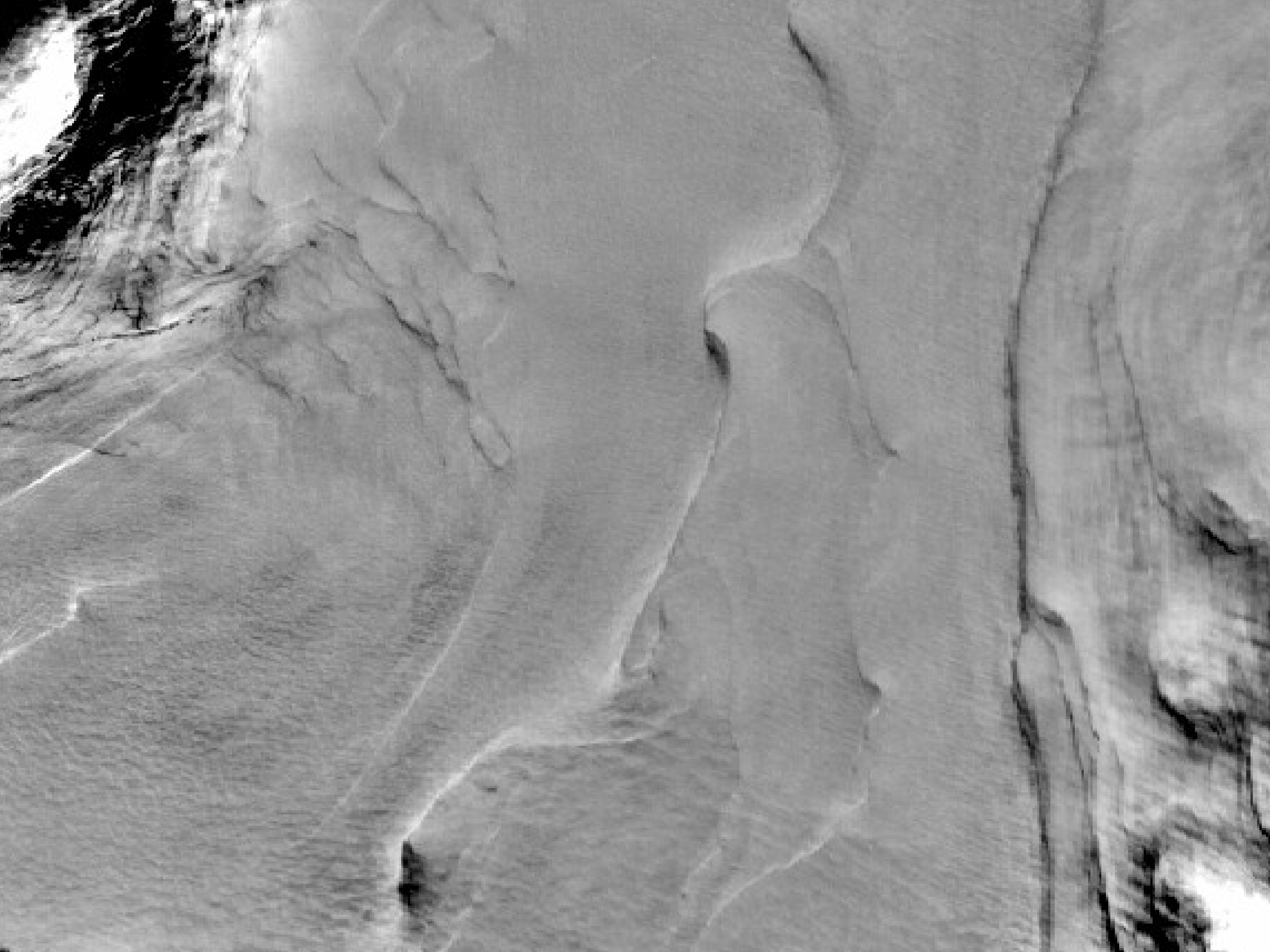

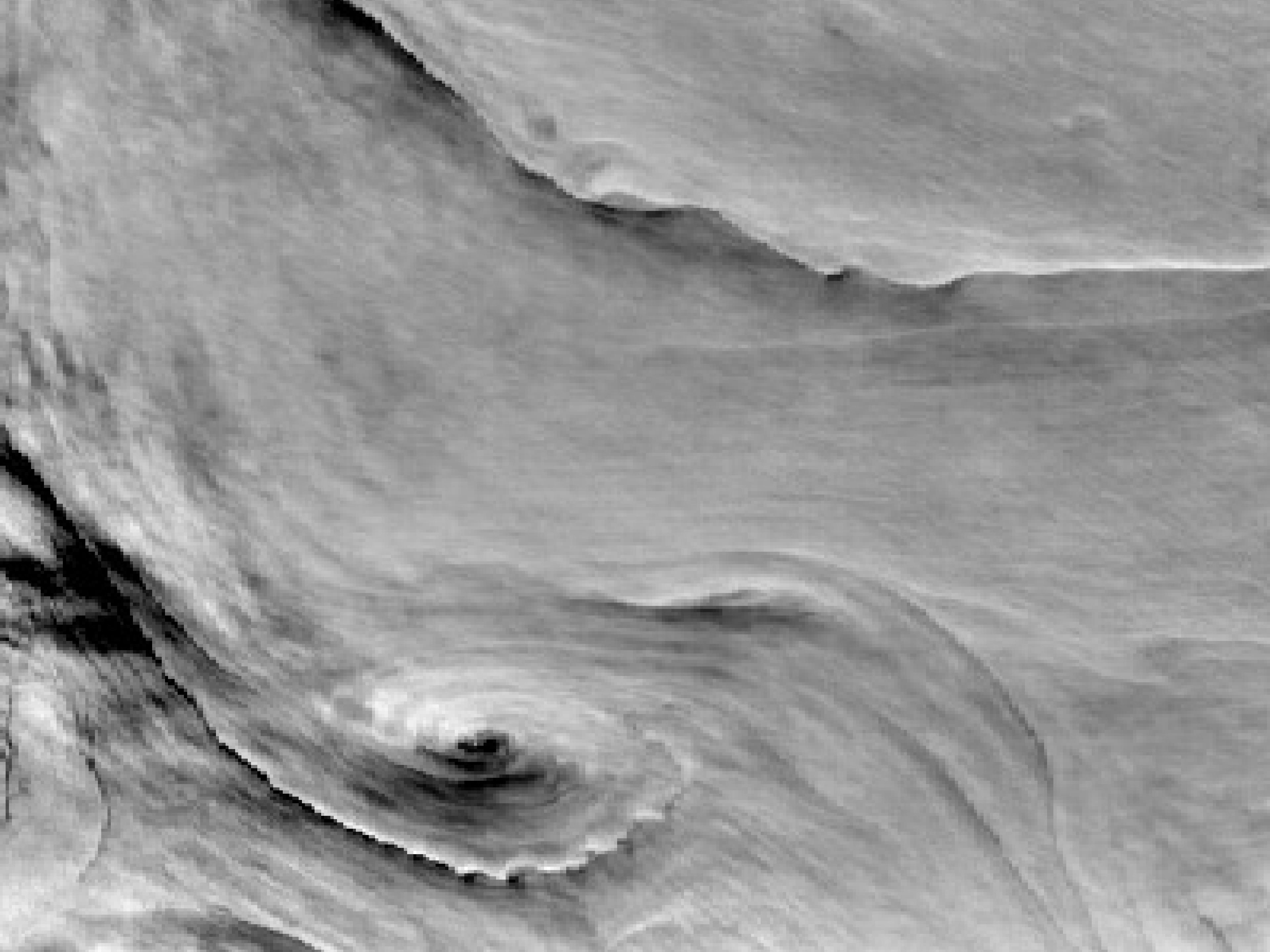

31Mar/07Apr (2010)
MODIS vs Altimetry-derived velocity field

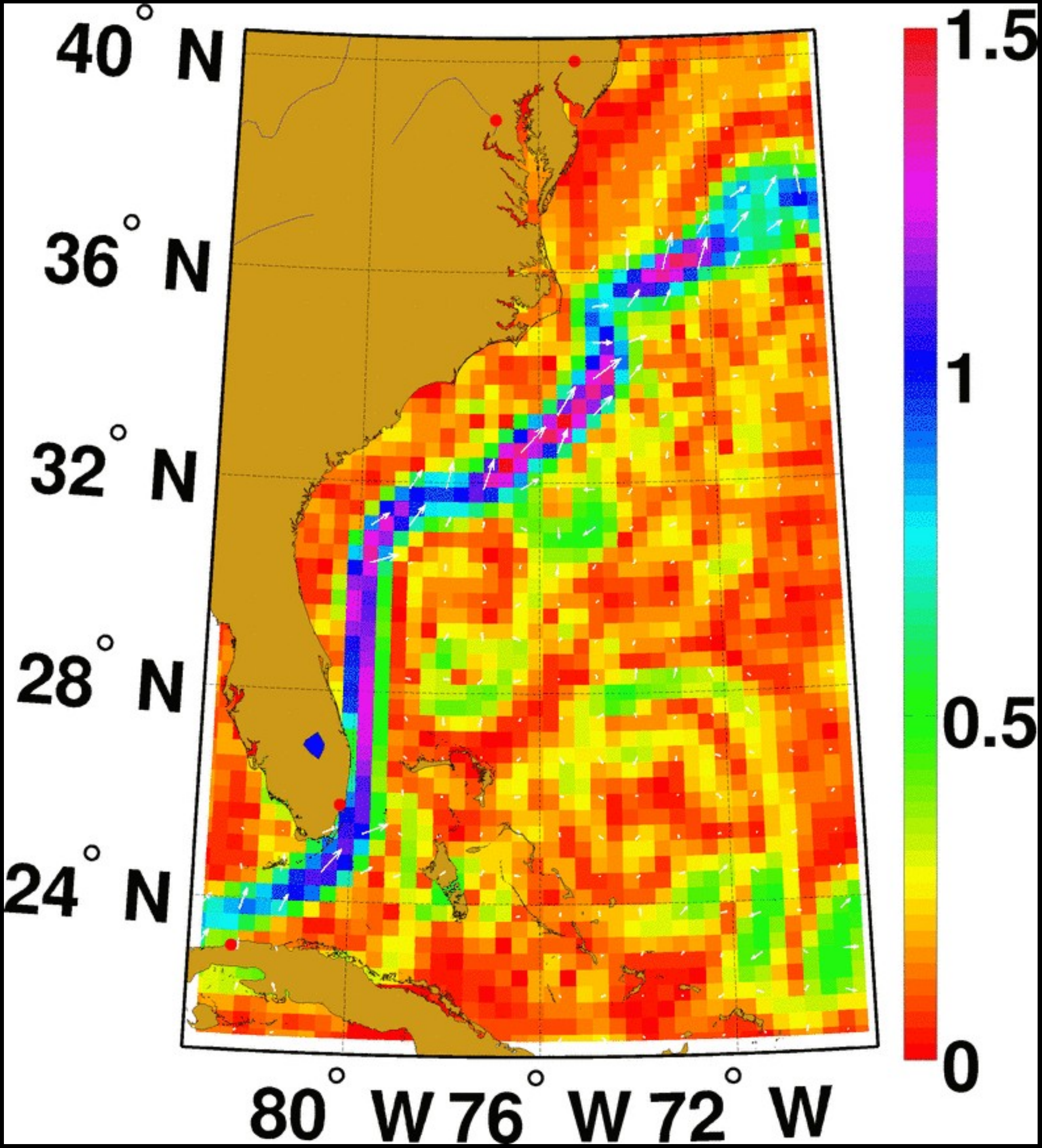

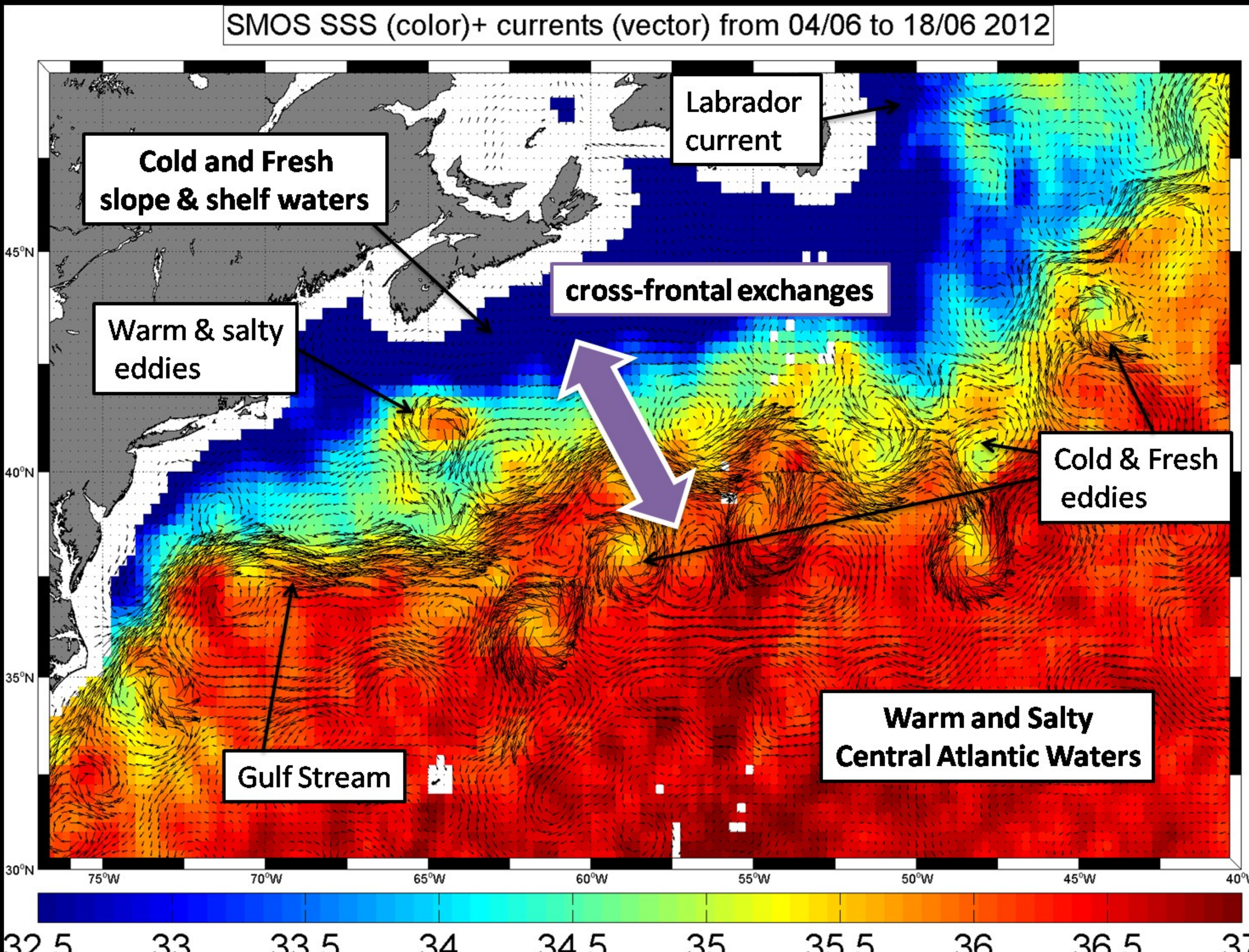
SMOS SSS (color)+ currents (vector) from 04/06 to 18/06 2012
Labrador current
Cold and Fresh slope & shelf waters
cross-frontal exchanges
Warm & salty eddies
Cold & Fresh eddies
Warm and Salty Central Atlantic Waters
Gulf Stream
45°N
40°N
35°N
30°N
75°W
70°W
65°W
60°W
55°W
50°W
45°W
40°W
32.5
33
33.5
34
34.5
35
35.5
36
36.5
37

Eastern Pacific Freshpool & 3D monitoring of the pool

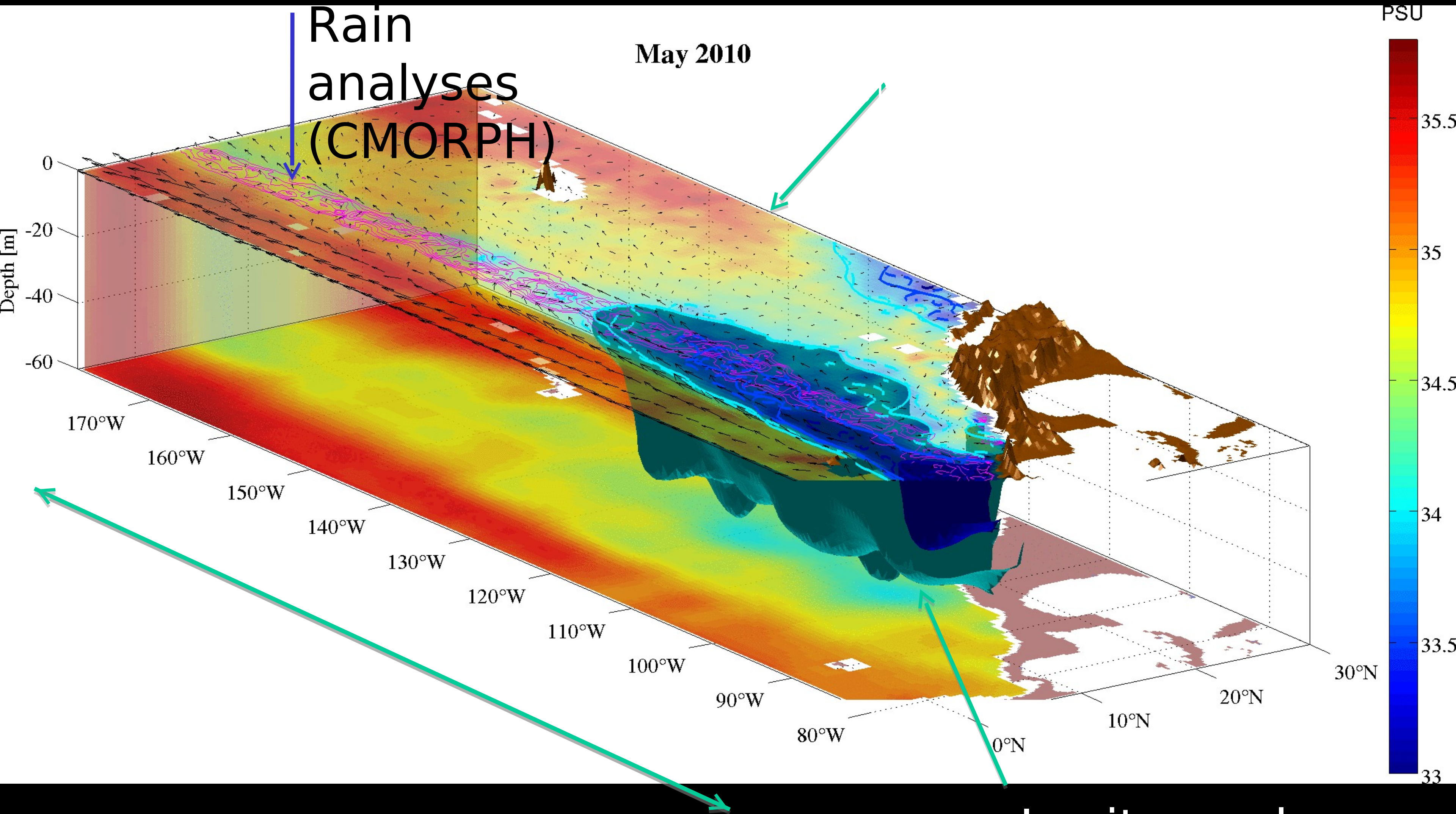

Application to Oil Spills Detection

Deepwater Horizon
May 24, 2010
Terra/MODIS

The blended satellite products allow to estimate the impact of surface currents on the biogeochemical transport, on the dispersion of pollutants and oil spills

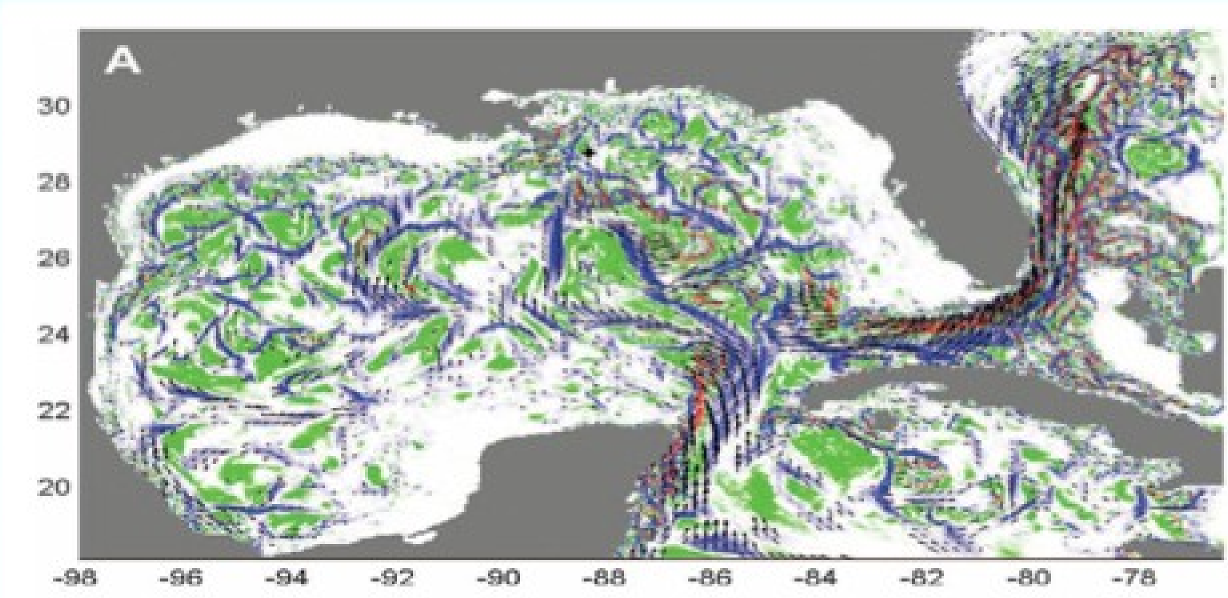

Forecast of oil spill dispersion in the Gulf of Mexico on 25 june 2010: red and blue show regions of strong oil dispersion within 3 days. This diagnosis, based on altimetric data, compared well with what was observed (Mezic et al, Science, 2010).

However these satellite datasets (altimetric and microwave data) cannot capture ocean dynamics at scales smaller than 100 km because of the resolution (or/and noise level).

Intense deformation field at oceanic front inferred from directional sea surface roughness observations

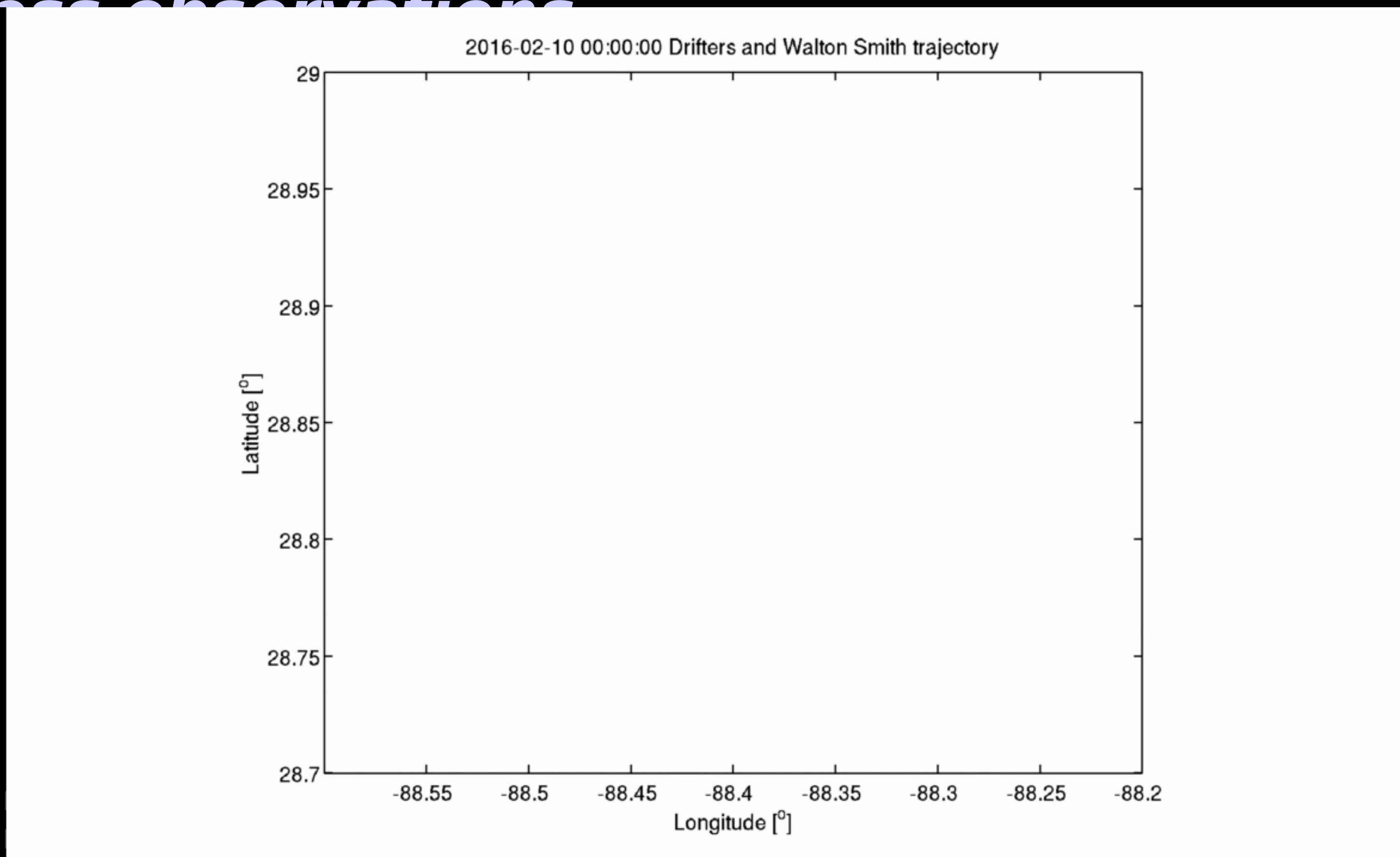

High resolution altimetry

mesoscale/submesoscale investigations

- **Should allow a characterization of submesoscale signals. Scales (wavelengths/2) between 10 and 100 km.**
- **Noise is a major issue (a goal of 1 cm / 1 km for an uncorrelated noise is quite challenging !).**
- **Time sampling will remain an issue for some applications.**

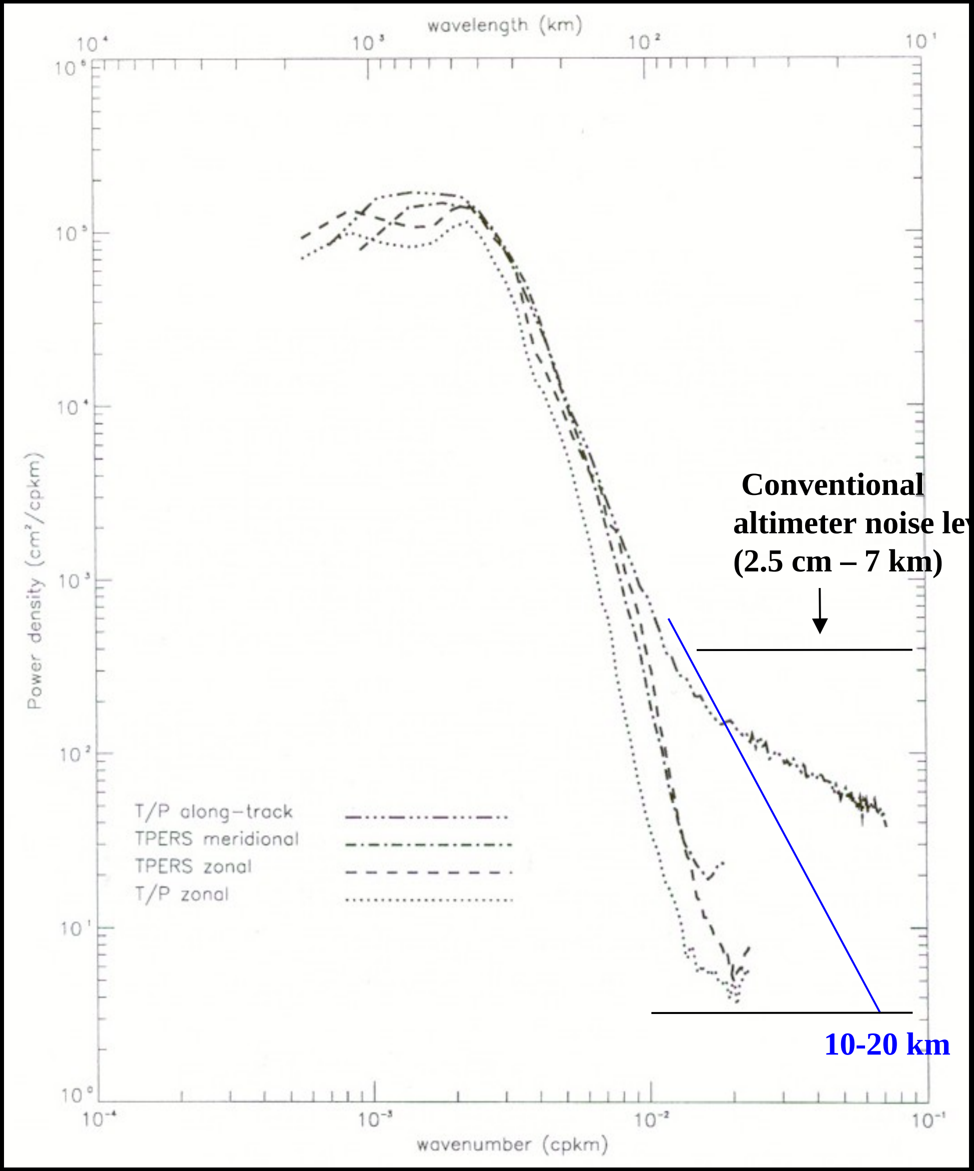

Ducet et al., 2000

Total Surface current vs altimetric currents

Kinetic energy spectra yields in the Gulf Stream region.

(Callies & Ferrari, 2013)

Present nadir altimetry is smoothed at scales < 100 km along-track

Differences in total surface currents and altimetry derived geostrophic currents are expected between 20-100 km => to explore with SWOT & total surface current obs

Gulf Stream : An interior QG–turbulence regime exists at large scales and an internal-wave regime at small scales, with the transition occurring at about 20 km.

Enhanced submesoscale energy may occur in the presence of a deep winter mixed layer

How does this vary, regionally, seasonally?

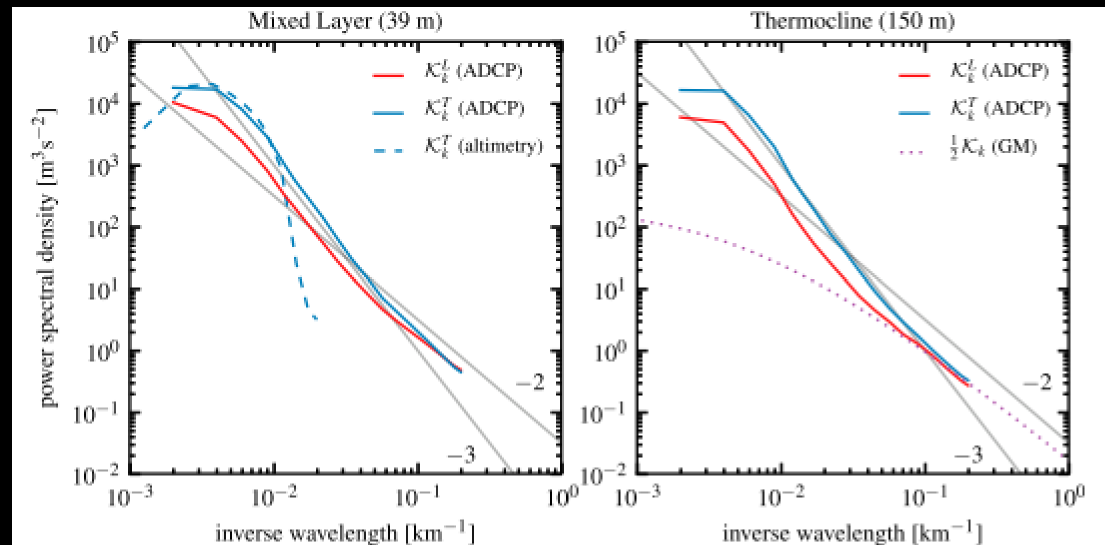

FIG. 5. Gulf Stream region wavenumber spectra of longitudinal and transverse kinetic energies $\mathcal{K}_k^L$ and $\mathcal{K}_k^T$ in the (left) mixed layer (39-m depth) and (right) thermocline (150-m depth) from in situ observations (ADCP). The wavenumber spectrum of surface transverse kinetic energy $\mathcal{K}_k^T$ from altimetry (left) and the GM model spectrum for kinetic energy $\mathcal{K}_k$ in the thermocline (right) are also shown. In both panels, lines with slopes −2 and −3 are given for reference (gray solid lines). Confidence intervals are too small to be visible.

APRIL 2010 NOTES AND CORRESPONDENCE

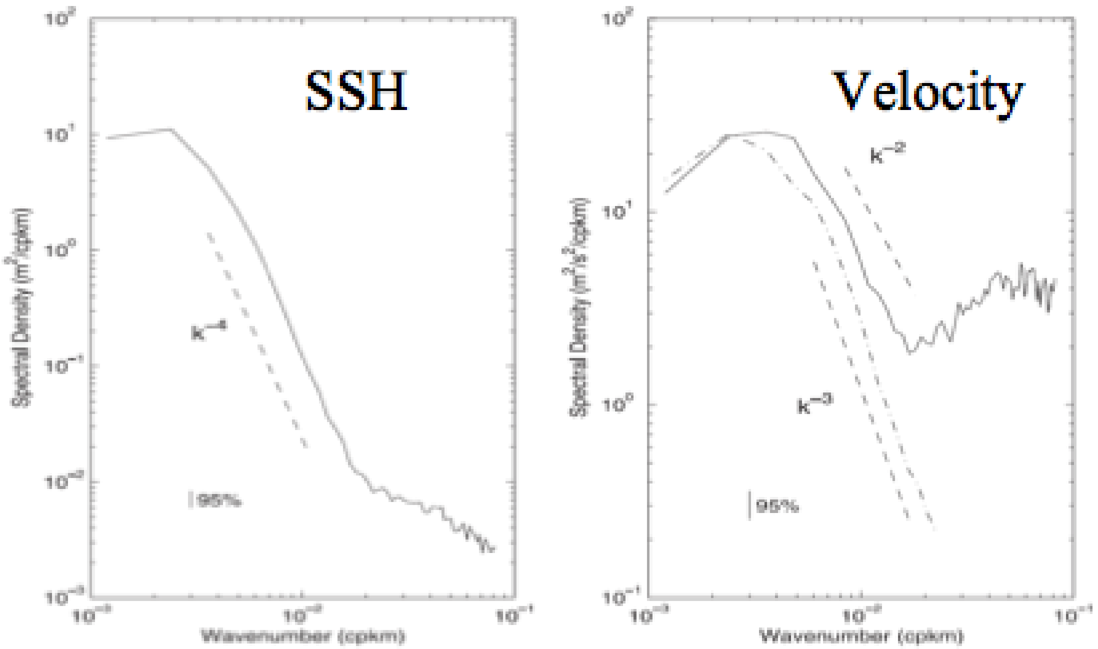

FIG. 3. (left) SSH and (right) geostrophic velocity spectra from altimetry measurements, superimposed with kinetic energy spectrum (dashed-dotted) from *Oleander* observations. Dashed lines indicate slopes of −4, −3, and −2, respectively. The 95% confidence interval is marked.

Wang et al., JPO 2010

Velocity spectrum: **k^{-3}** from **ADCP data** (*Oleander* dataset) **steeper than k^{-2}** from **SSH**

Kinetic energy: **smaller energy** level with ADCP data than altimetric data

Temperature spectrum: $k^{-2.3}$ (closer to velocity spectrum from SSH)

We hypothesize that vertical mixing within the ML explains the departure of surface currents from geostrophy

$$-f\boldsymbol{k}\times\boldsymbol{u}_{ml} - \frac{\partial}{\partial z}A_v\frac{\partial \boldsymbol{u}_{ml}}{\partial z} = -\frac{1}{\rho_o}\boldsymbol{\nabla} p$$

Coriolis term

Wind-forced mixing

Pressure (ssh) gradients forced by eddy turbulence

After integration over the mixed-layer depth (using the SQG approximation for p), we get :

$$\widehat{\boldsymbol{u}_e}(k_x,k_y) = \widehat{\boldsymbol{u}_g}(k_x,k_y,0)\frac{f}{kNH}[1-exp(\frac{-kNH}{f})]$$

Surface currents

Geostrophic currents (from SSH)

Wind-forced ML depth

Discovering Ocean Dynamics from Space: several strategies

- Numerous Remote sensing measurements to invite feature tracking techniques (e.g. MCC, optical-flow methods)
  - Very high resolution (100 m – 1 km) SST, Ocean Colour, radar and optical roughness images
  - Low resolution Altimetry (80 km)
  - Mesoscale Ocean Wind Vector Scatterometry and Microwave SST and SSS (25 km)

- Increased In Situ measurements
  - Fixed networks, ARGO floats, drifters, ship tracking

- Dynamical frameworks
  - Operational models, Quasi-geostrophy, Surface Quasi-geostropy
  - Ekman, wave-induced Stokes drift
  - Swell system anomalous propagations

Sentinel-2 MSI Features = New Opportunities to image ocean surface waves and dispersion properties

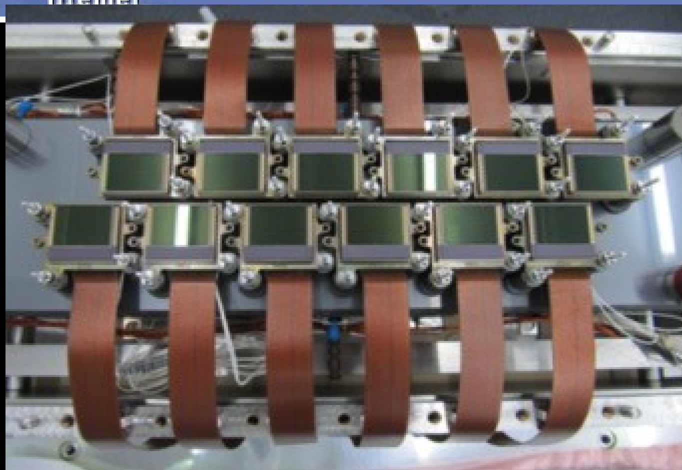

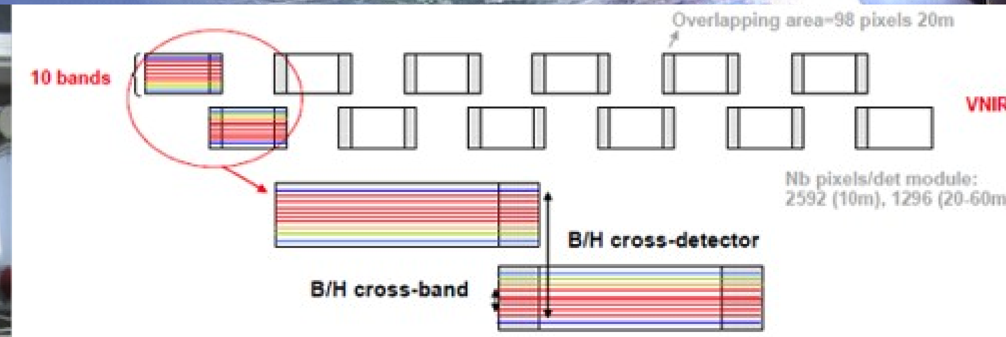

Sentinel-2 detectors

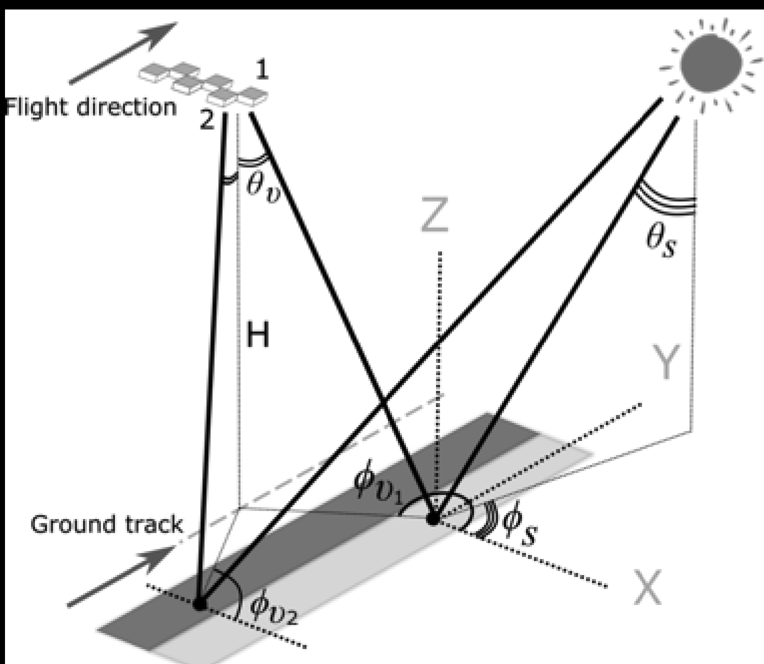

12 clusters (detectors), 13 lines of sensors (bands) in each

Odd clusters are looking forward, even clusters are looking backward, spectral channel sensors also have relative displacement

Parallax angle between the two alternating odd and even clusters of detectors results in a shift along track of approximately 46 km (maximum).

Inter-band measurement parallax amounts to a maximum along track displacement of approximately 14 km.

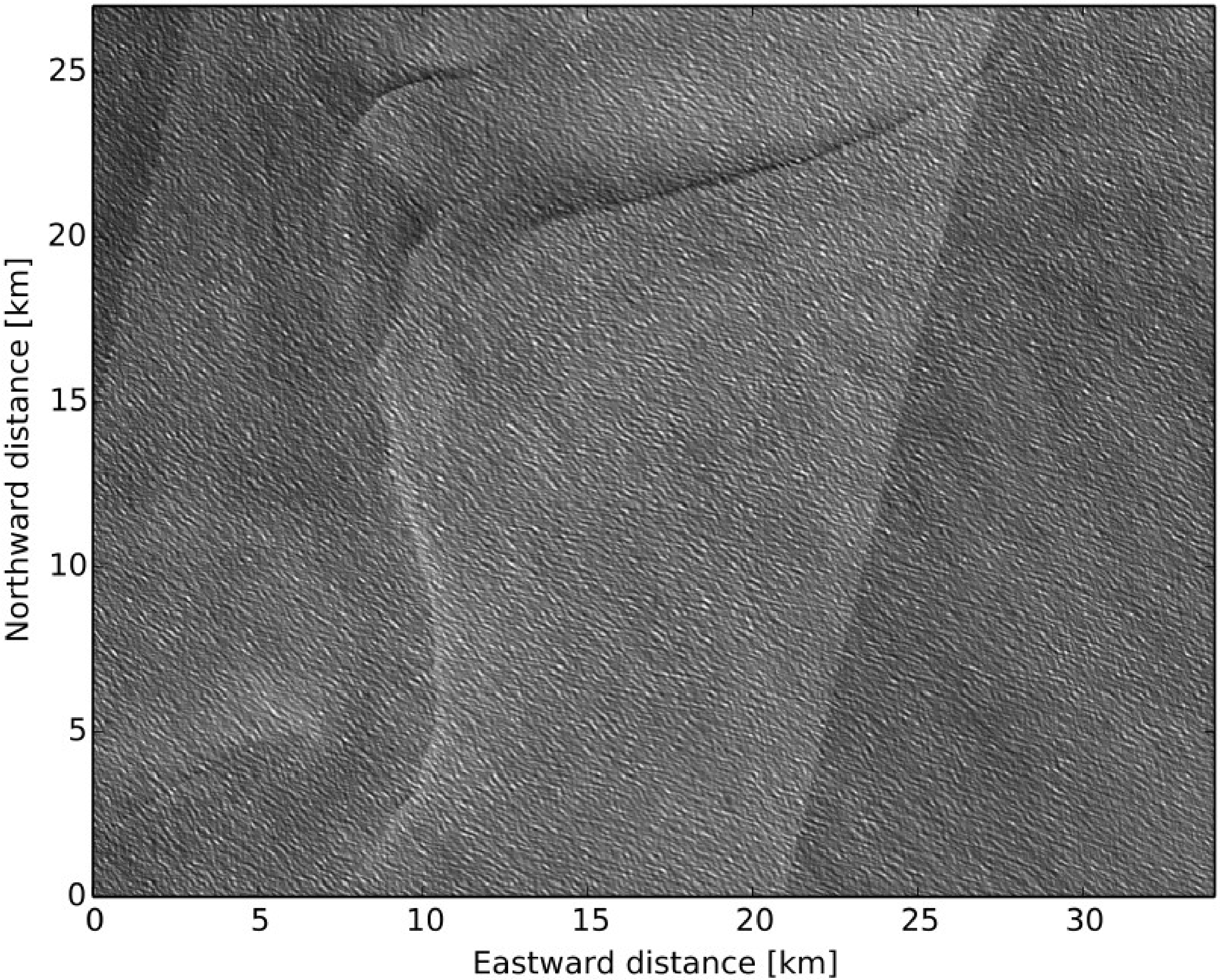

Northward distance [km]
Eastward distance [km]
0
5
10
15
20
25
30

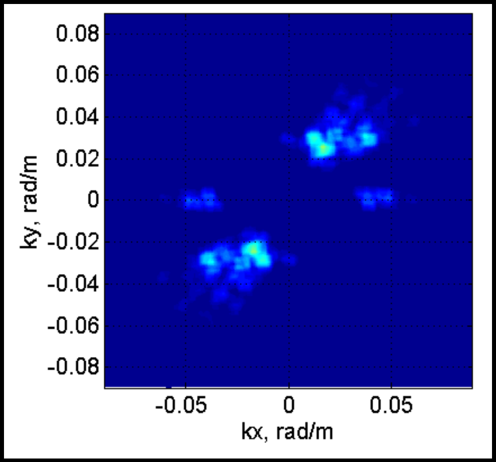

0.08
0.06
0.04
0.02
0
-0.02
-0.04
-0.06
-0.08
ky, rad/m
-0.05
0
0.05
kx, rad/m

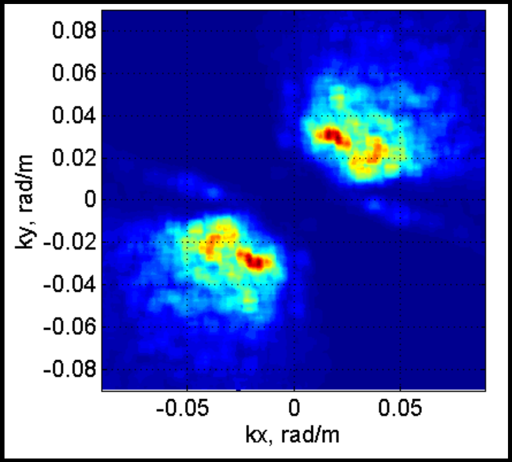

0.08
0.06
0.04
0.02
0
-0.02
-0.04
-0.06
-0.08
ky, rad/m
-0.05
0
0.05
kx, rad/m

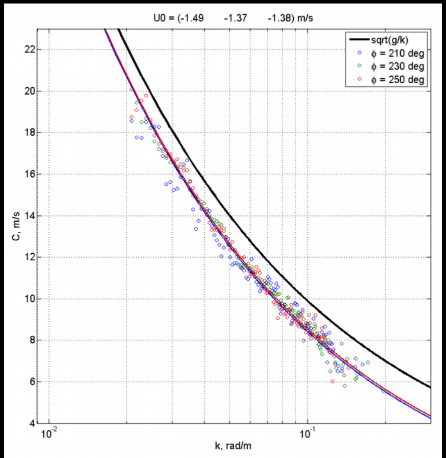

U0 = (-1.49 -1.37 -1.38) m/s
sqrt(g/k)
ϕ = 210 deg
ϕ = 230 deg
ϕ = 250 deg
C, m/s
k, rad/m

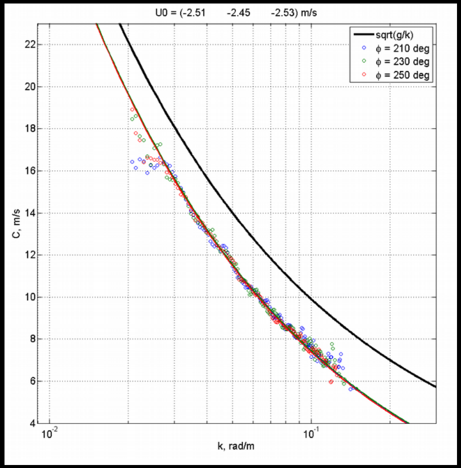

U0 = (-2.51 -2.45 -2.53) m/s
sqrt(g/k)
ϕ = 210 deg
ϕ = 230 deg
ϕ = 250 deg
C, m/s
k, rad/m

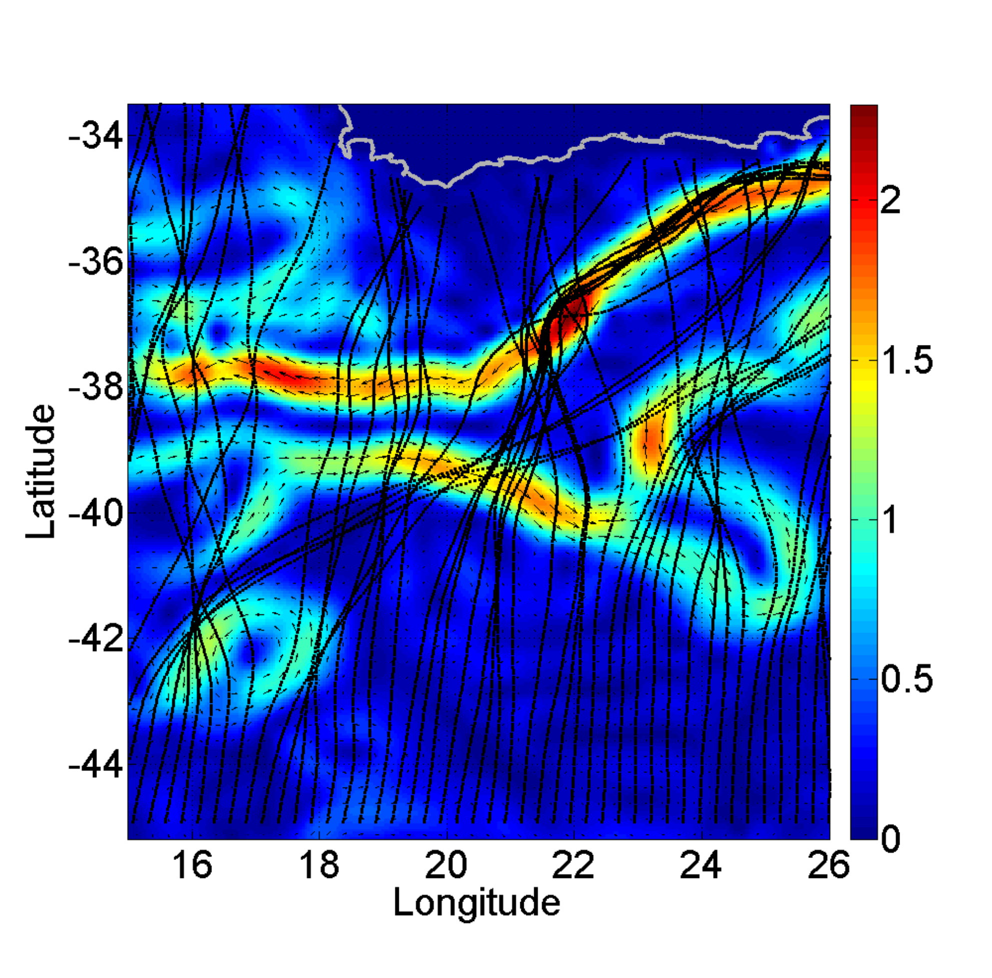

Wave-rays of an incoming 75 degree (counter clockwise from the East) 250 m swell at -45 degree latitude,

Gulf Stream roughness changes

Gulf Stream roughness changes

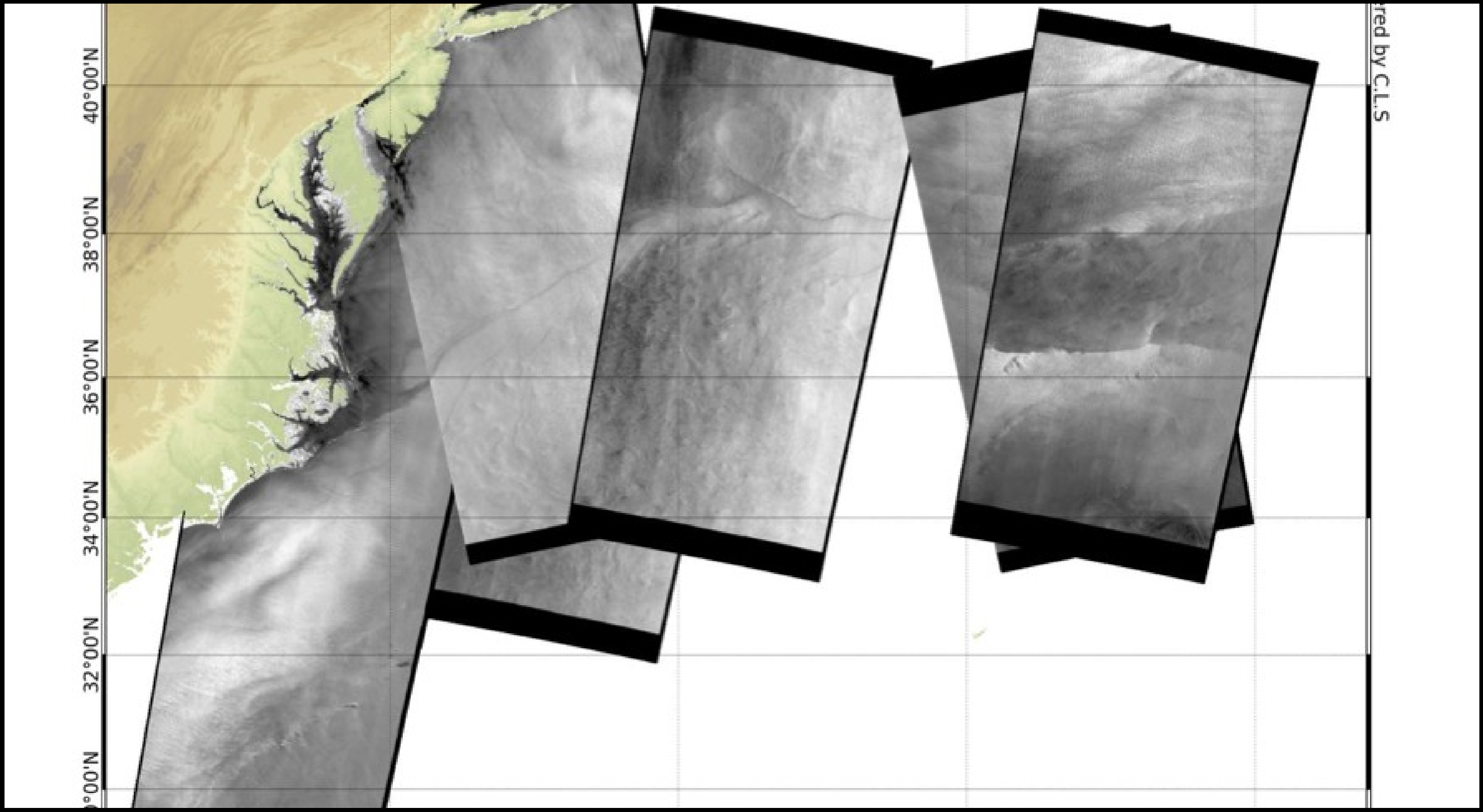

Meso-scale Air-Sea Interactions (High-pass filtered surface wind speed)

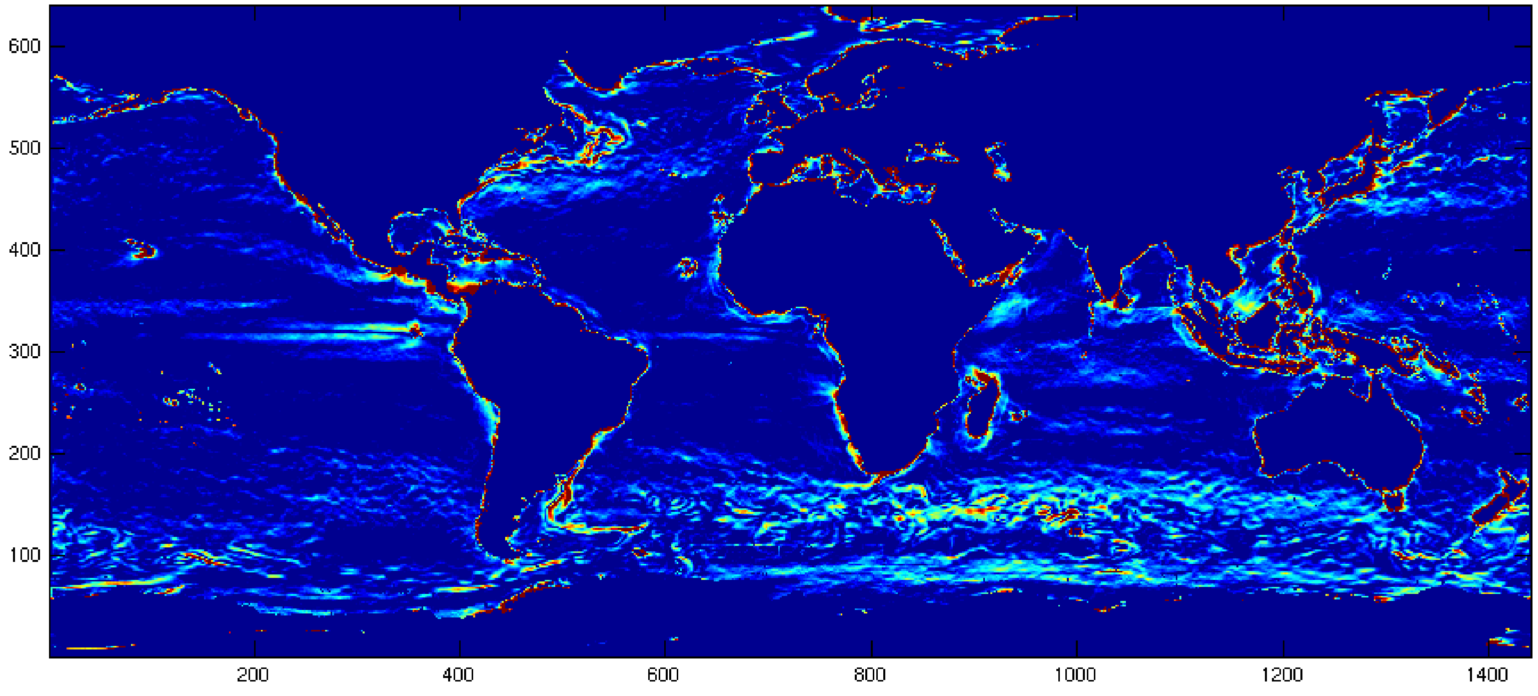

Meso-scale Air-Sea Interactions
Mean scatterometer wind-product curl (Chelton et al., 2007)

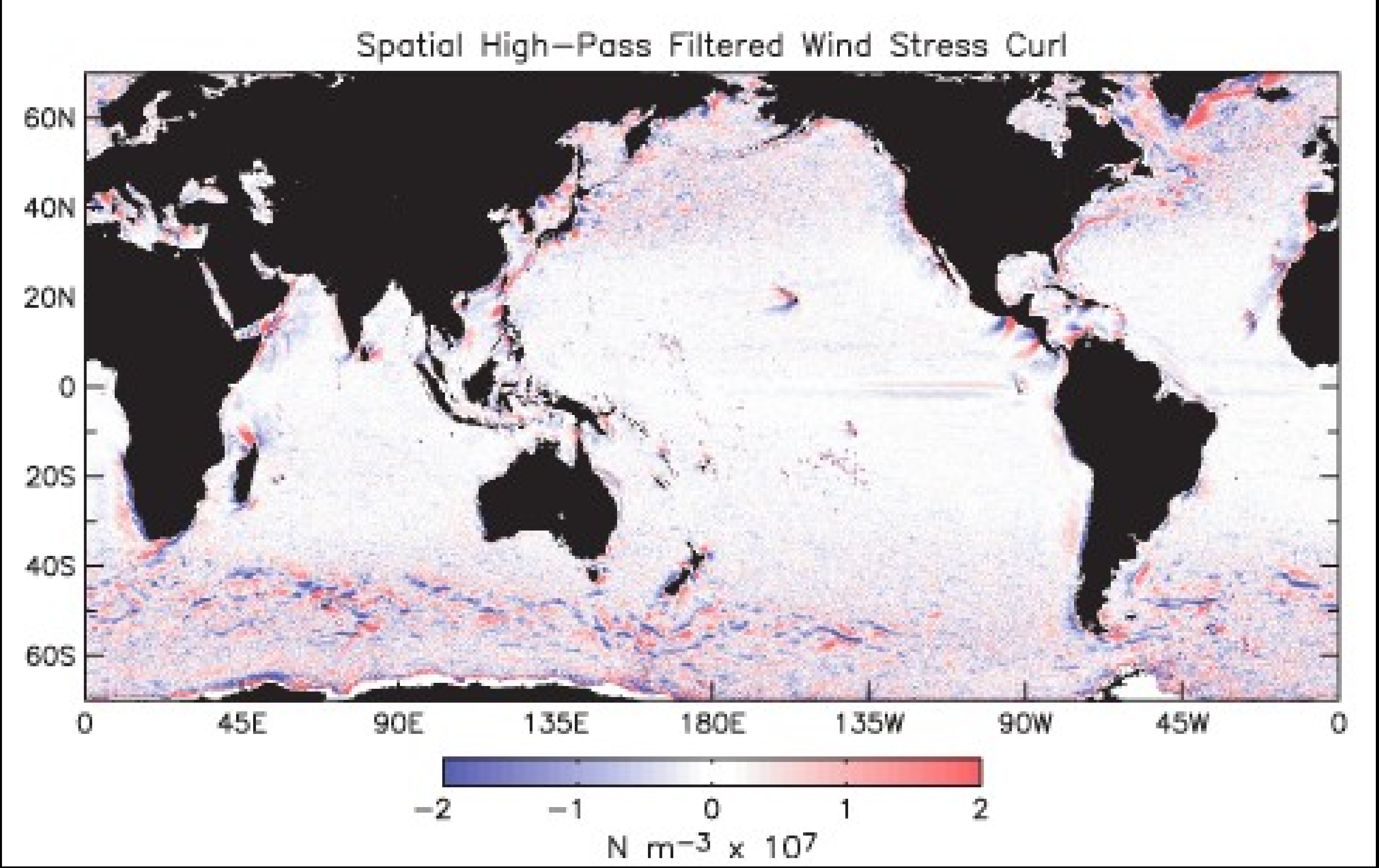

$$u_p = |u| * \cos(\phi_{buoycurr} - \phi_{buoywind})$$

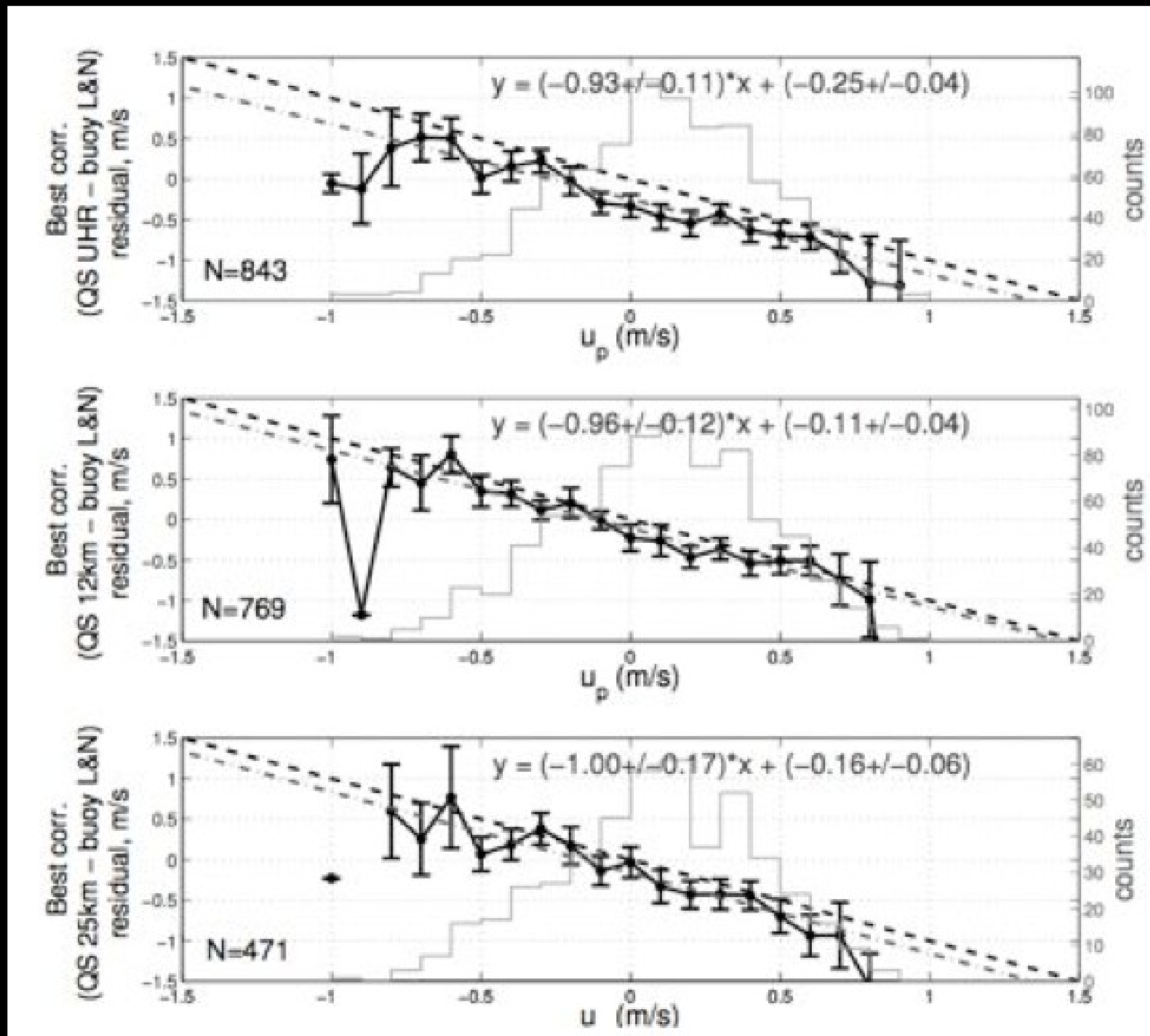

Coupled Ocean-Atmosphere system: Eddy/wind interactions , i.e. the nonlinear Ekman effects

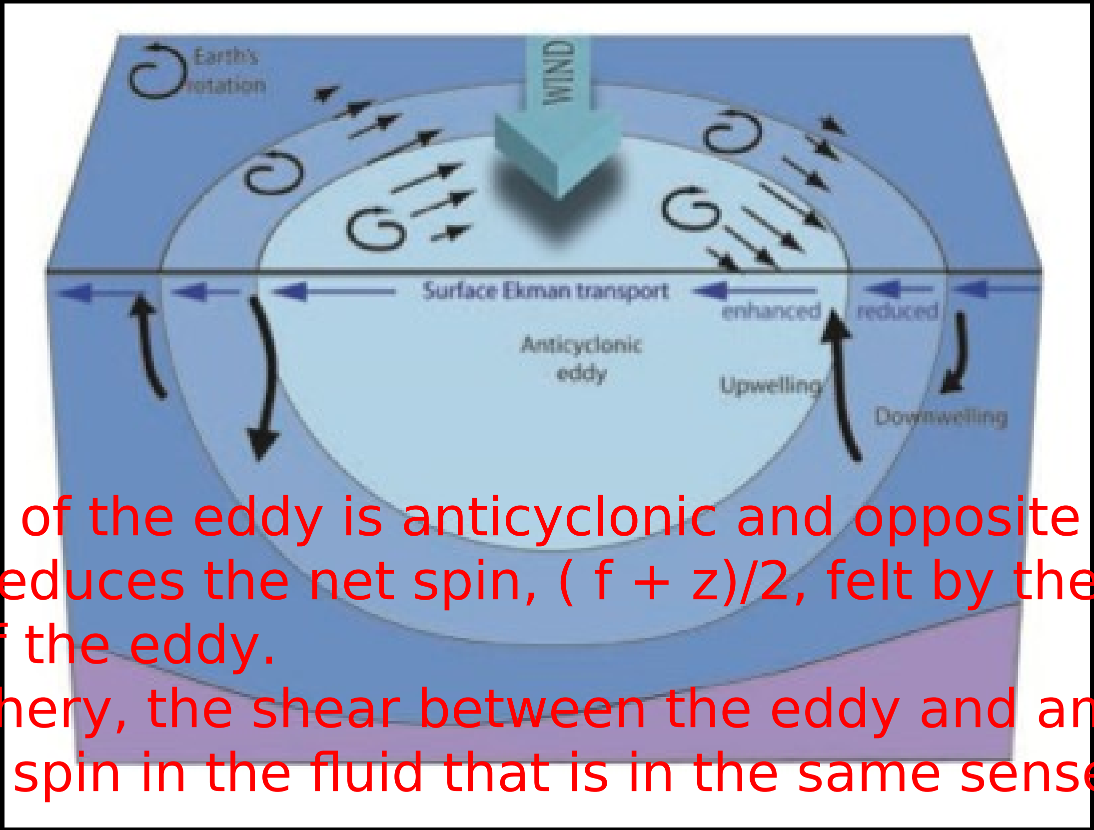

The rotation of the eddy is anticyclonic and opposite to Earth’s rotation. It reduces the net spin, $(f + z)/2$, felt by the fluid toward the inside of the eddy.

At the periphery, the shear between the eddy and ambient fluid generates a spin in the fluid that is in the same sense as Earth’s rotation

The divergence/convergence of the Ekman transport can then drive alternate up/down motions

Sea Surface Roughness (SSR) dynamical variations

$$\frac{\partial N(\mathbf{k})}{\partial t} + \left(c_{gi} + u_i\right)\frac{\partial N(\mathbf{k})}{\partial x_i} - k_j \frac{\partial u_j}{\partial x_i}\frac{\partial N(\mathbf{k})}{\partial k_i} = Q(\mathbf{k})/\omega$$

$$Q(\mathbf{k}) = \beta_\nu(\mathbf{k})\omega E(\mathbf{k}) - D(\mathbf{k}) - Q^{nl}(\mathbf{k}) + Q^{wb}(\mathbf{k})$$

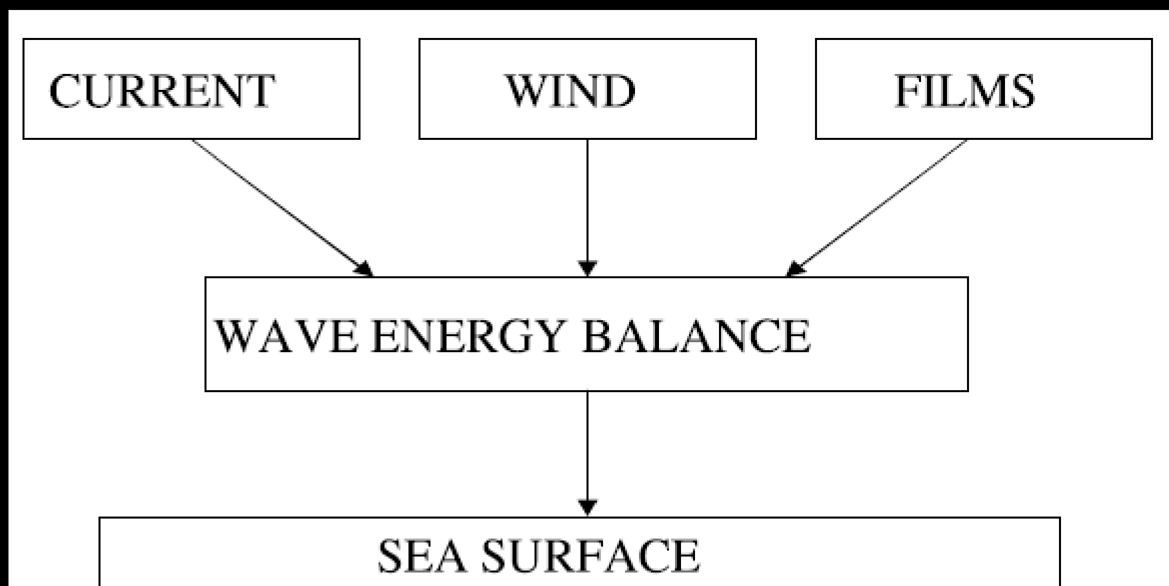

$$\partial\tilde{N}(\mathbf{k})/\partial t + c_{gi}\partial\tilde{N}(\mathbf{k})/\partial x_i = \omega^2 k^{-5}\left[\omega^{-1} m_k^{ij} u_{i,j} B_0 - \tilde{B}/\tau + \tilde{\beta} B_0 + \tilde{I}_{sw}\right]$$

$$m_k^{ij} = k_j \partial \ \ln \ N_0/\partial k_i$$

Direct ocean surface Doppler velocities from space

SRTM 2-Antenna Interferometry

Ultra-high resolution
Limited to line-of-sight direction

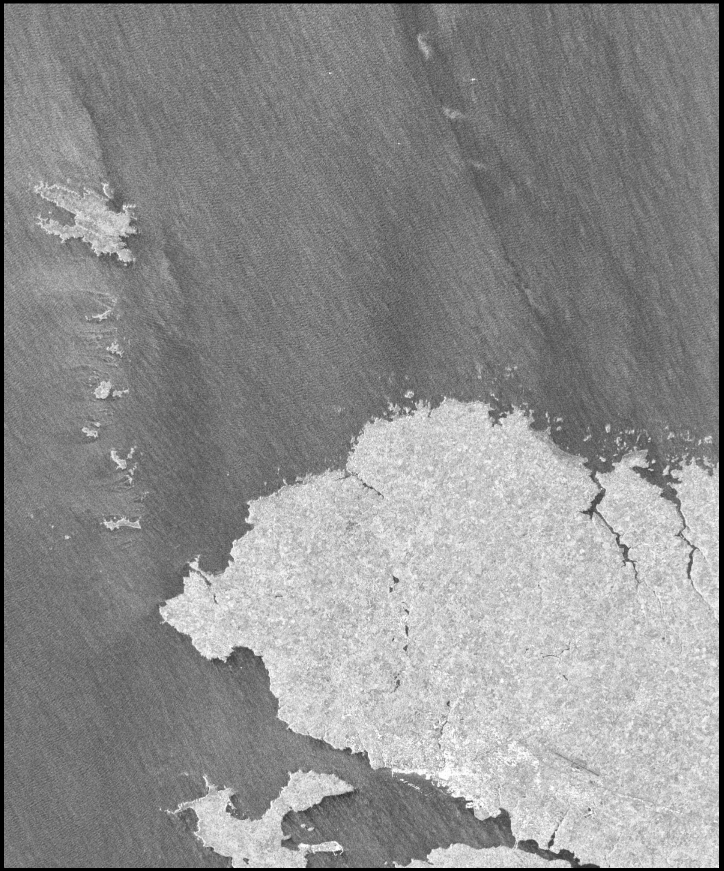

To obtain direct ocean surface velocities from space

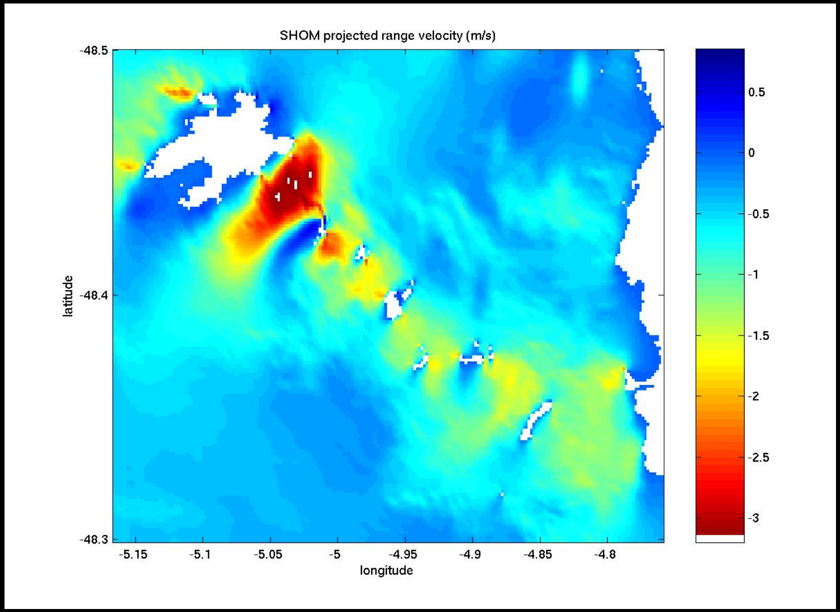

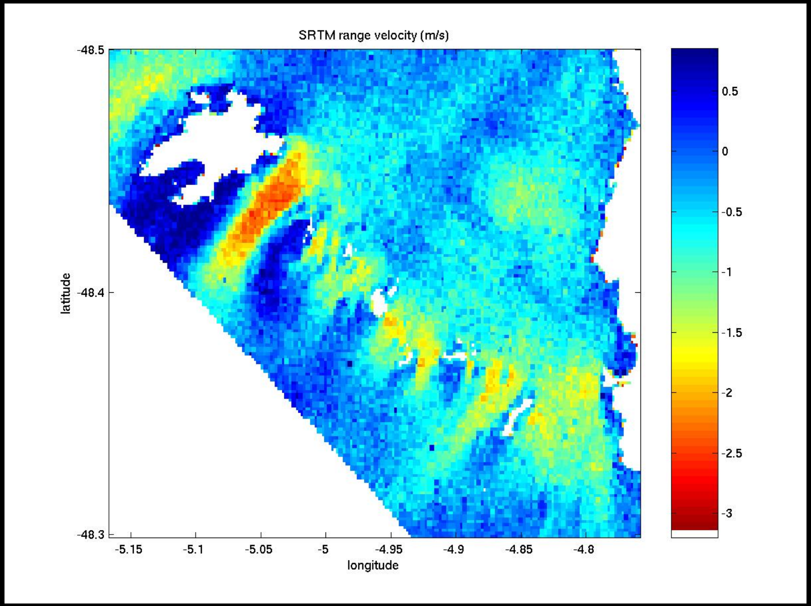

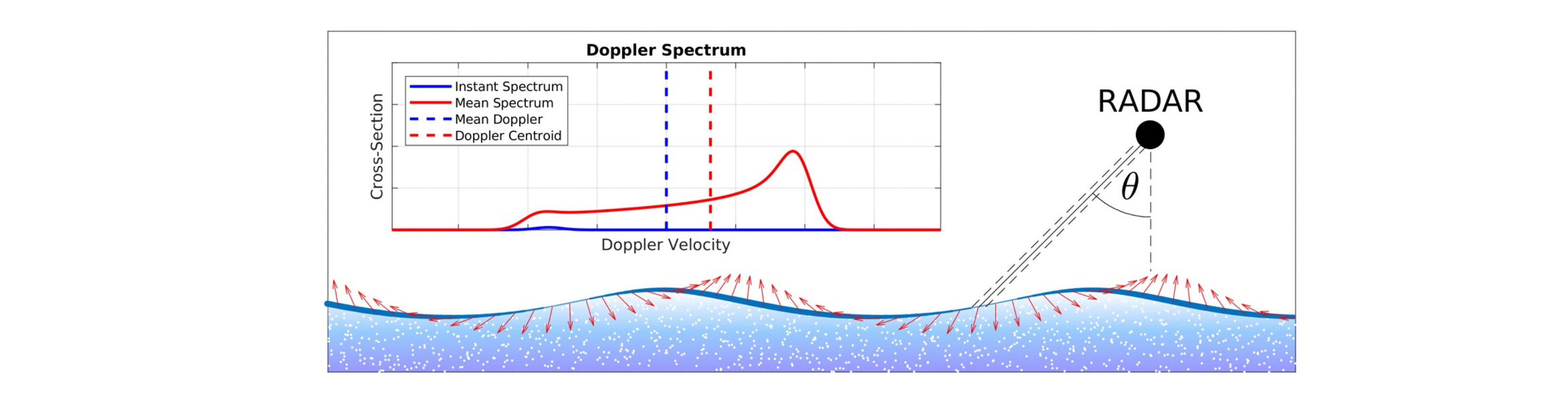
Doppler Spectrum
Instant Spectrum
Mean Spectrum
Mean Doppler
Doppler Centroid
Cross-Section
Doppler Velocity
RADAR
θ

APPROACH: Combined Roughness and Doppler Shift

$\sigma_0(\vartheta) = \sigma_0$ (surface roughness) =
σ_0(wind, waves, breaking, curr

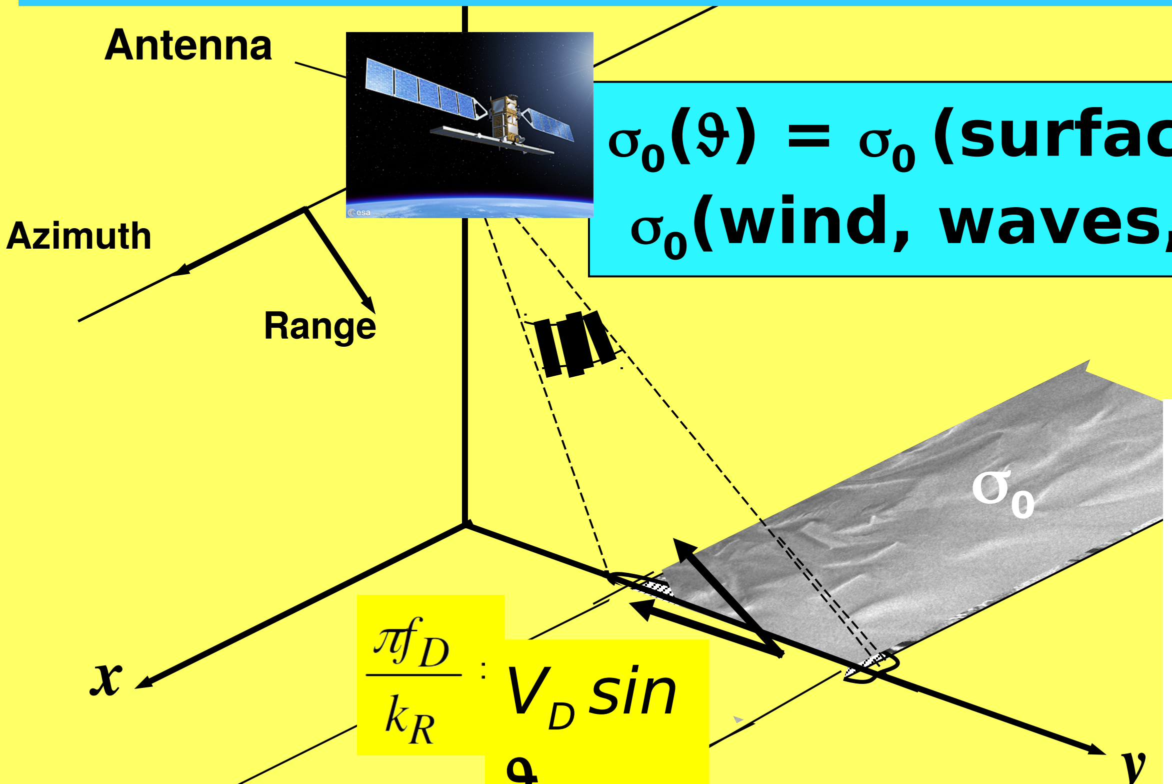

$$\frac{\pi f_D}{k_R} : V_D \sin \vartheta$$

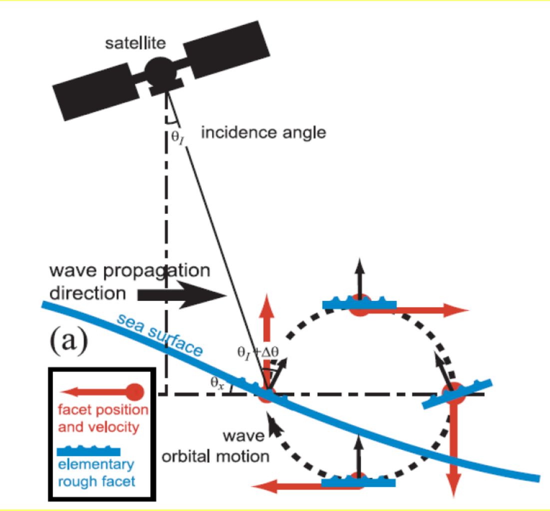

$V_D = V_D$ (wind driven scatterer, waves, breaking, current)

doppler centroid anomaly

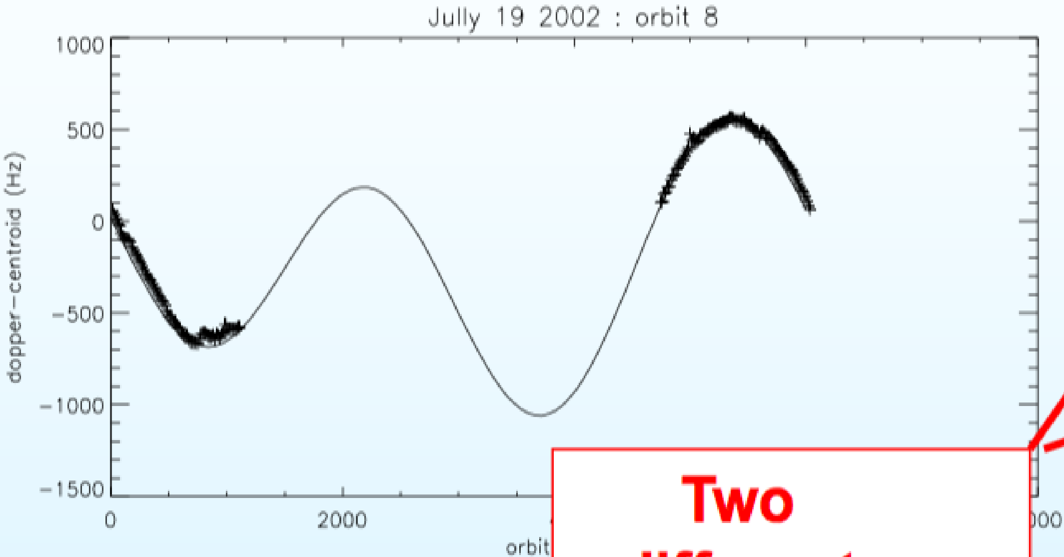

Two different tracks

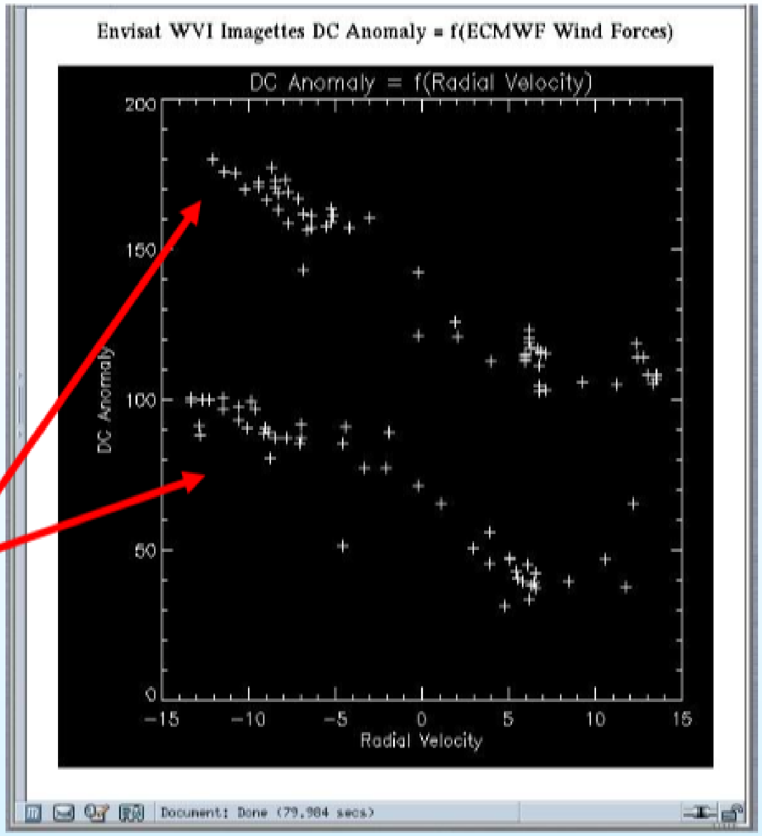

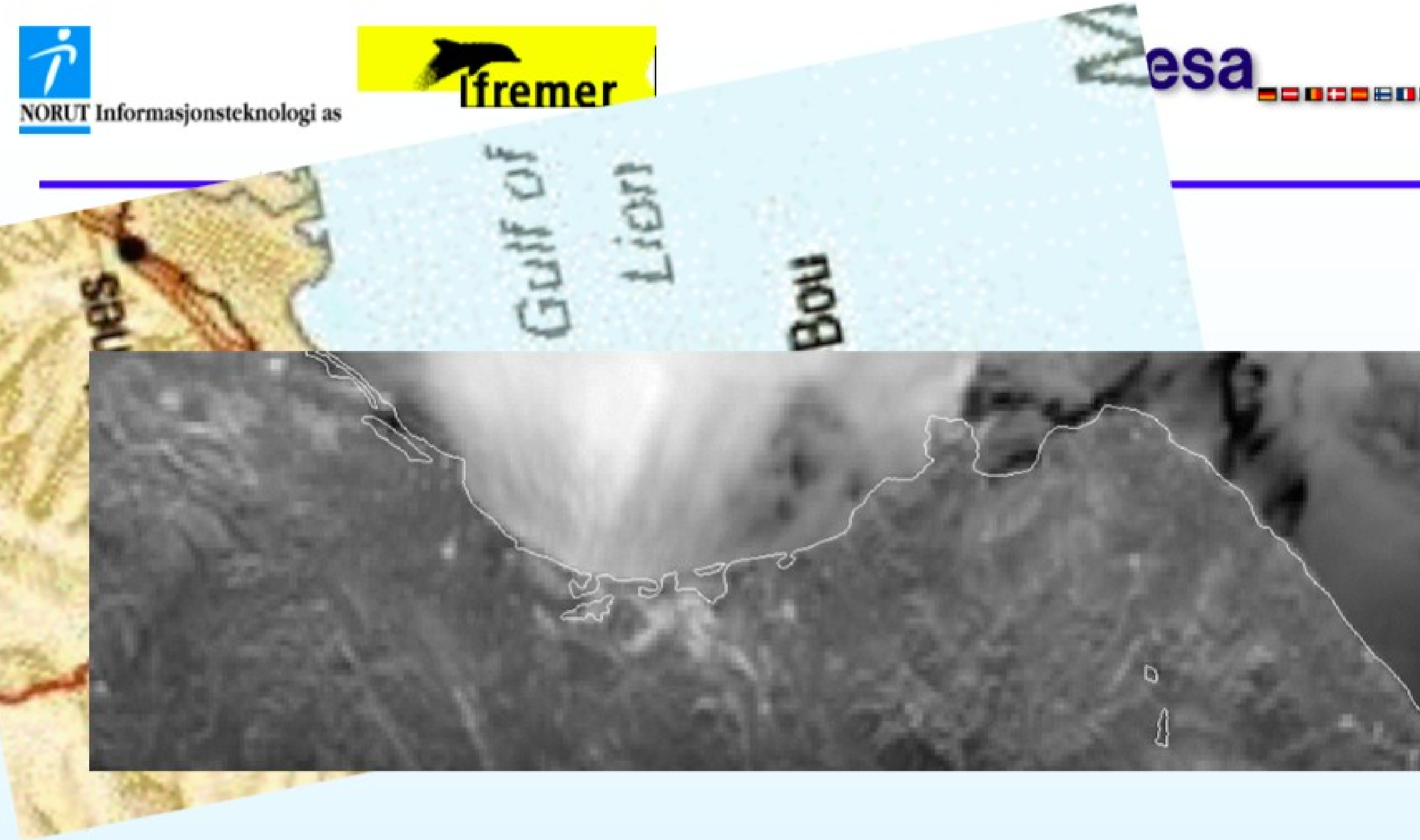

Comparison with a similar ERS 2 SLC image
doppler centroid analysis

Doppler anomaly chart

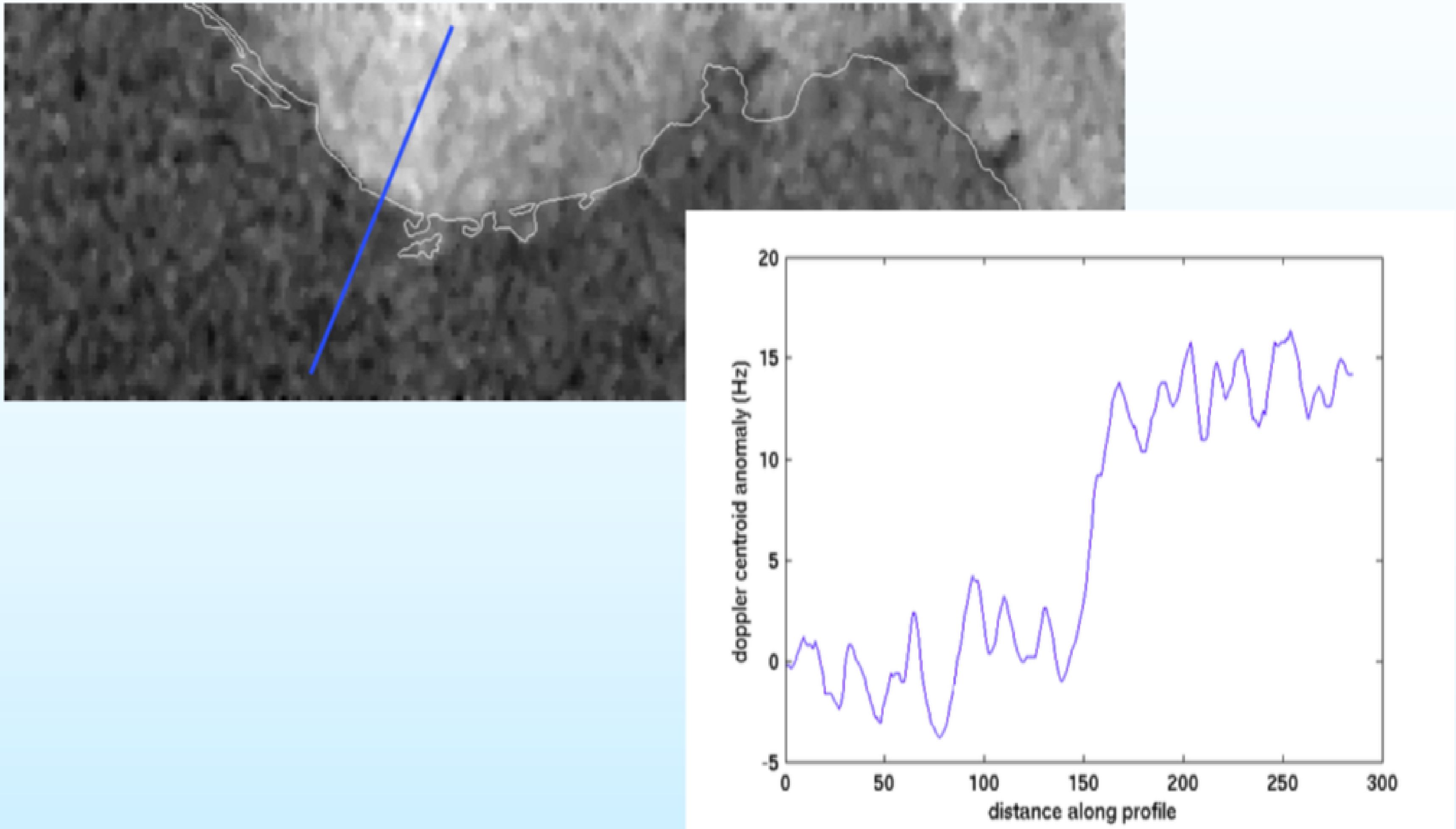

Doppler centroid anomaly on Wave mode level1b (descending tracks)

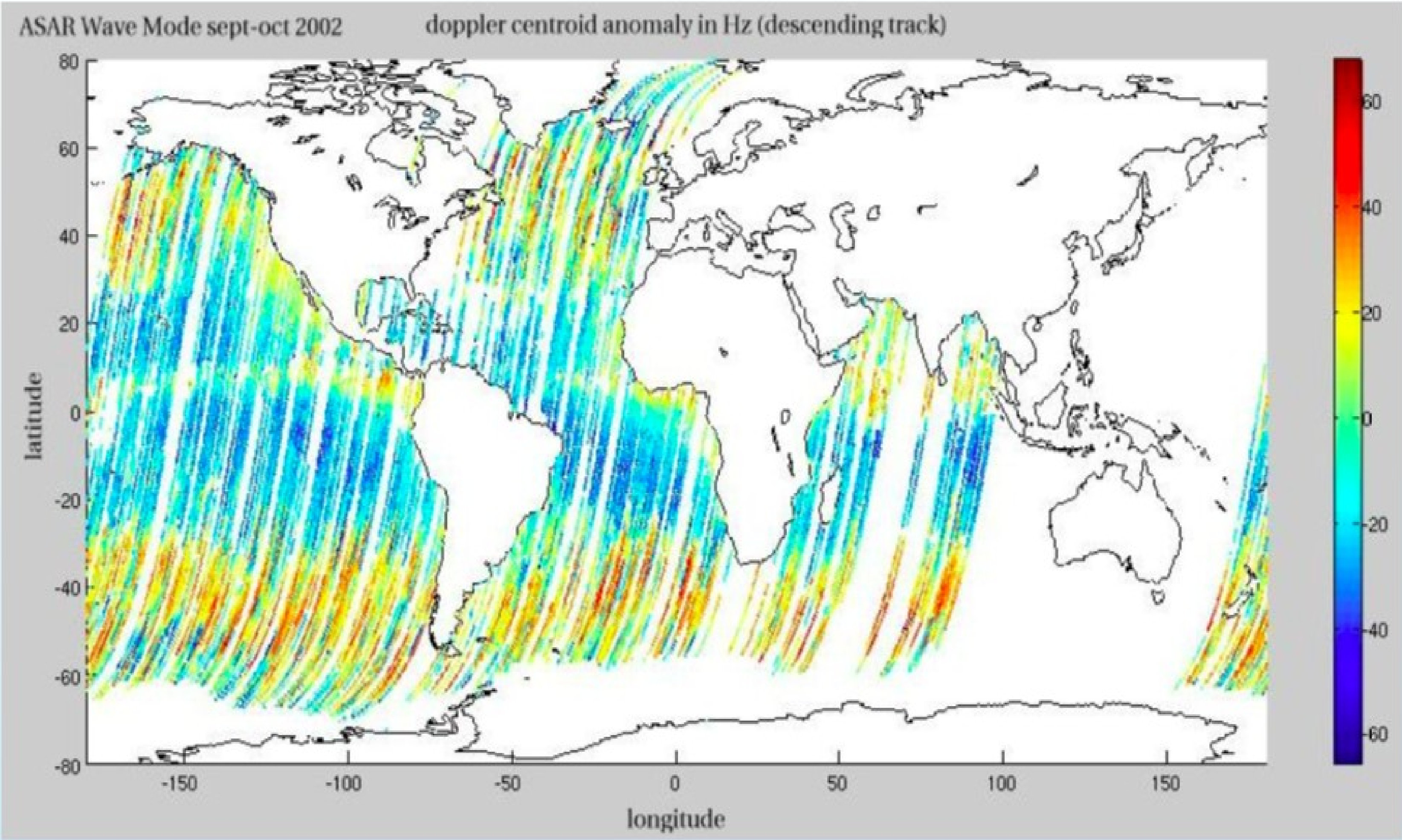

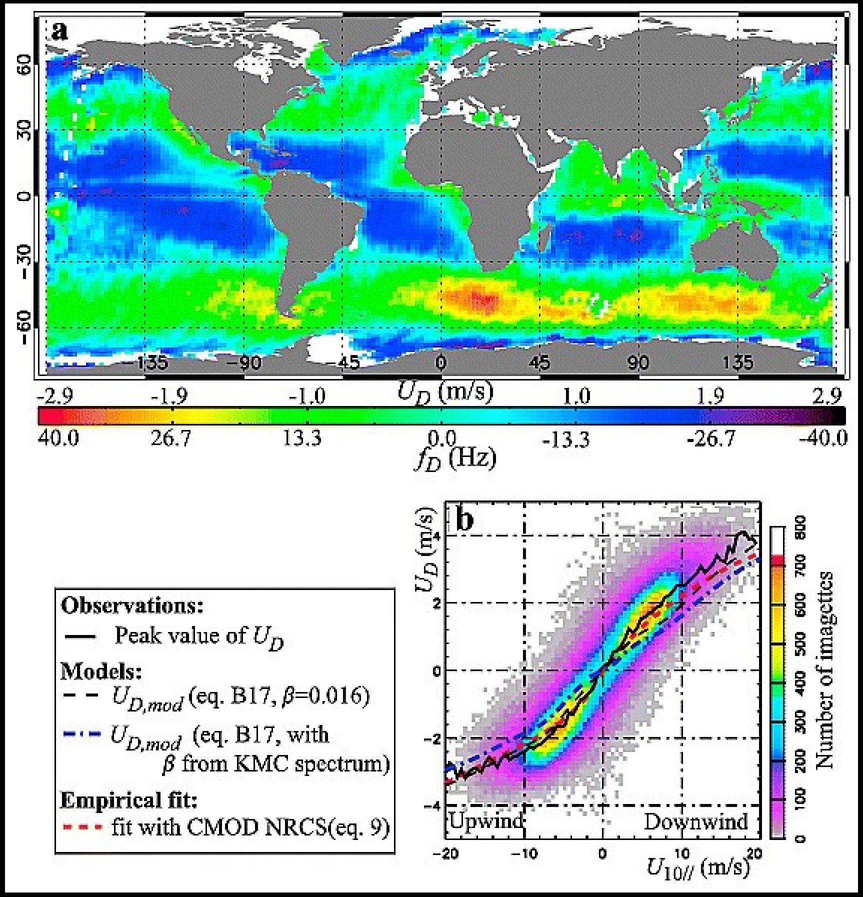
a
60
30
0
-30
-60
-135
-90
-45
0
45
90
135
-2.9
-1.9
-1.0
U_D (m/s)
1.0
1.9
2.9
40.0
26.7
13.3
0.0
-13.3
-26.7
-40.0
f_D (Hz)
b
U_D (m/s)
Observations:
Peak value of U_D
Models:
$U_{D,mod}$ (eq. B17, β=0.016)
$U_{D,mod}$ (eq. B17, with β from KMC spectrum)
Empirical fit:
fit with CMOD NRCS(eq. 9)
Upwind
Downwind
-20
-10
0
10
20
$U_{10//}$ (m/s)
Number of imagettes

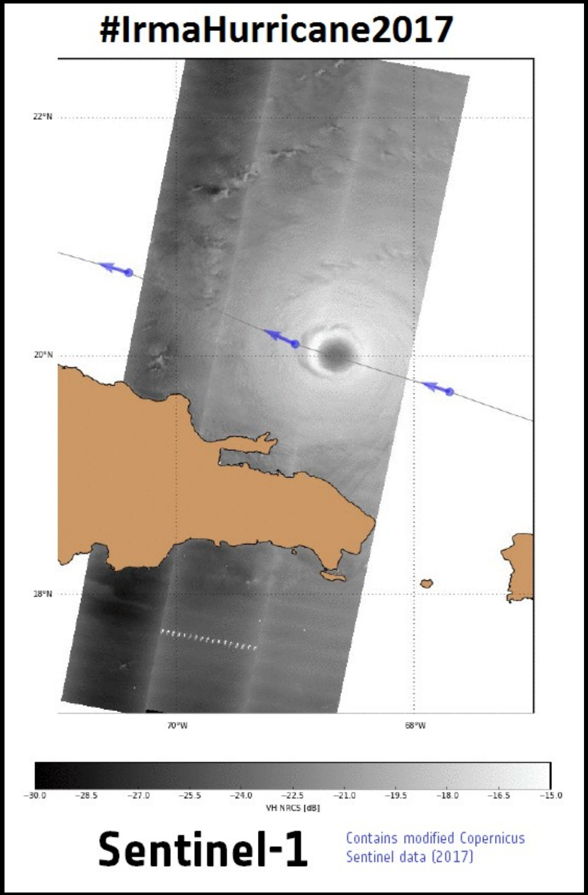
#IrmaHurricane2017
22°N
20°N
18°N
70°W
68°W
VH NRCS [dB]
Sentinel-1
Contains modified Copernicus
Sentinel data (2017)

As for Envisat/ASAR, Sentinel-1 A & B are the only missions able to routinely provide Doppler anomalies.

In addition, Sentinel-1 SAR provide Doppler at 1 km and in both VV and VH polarizations.

First analysis of data acquired over hurricane reveal that:

- Doppler in VV and VH have a very similar behaviour
- They do not saturate at high winds reaching Doppler values larger than 100 Hz
- They are very sensitive to the wind direction relative to the antenna

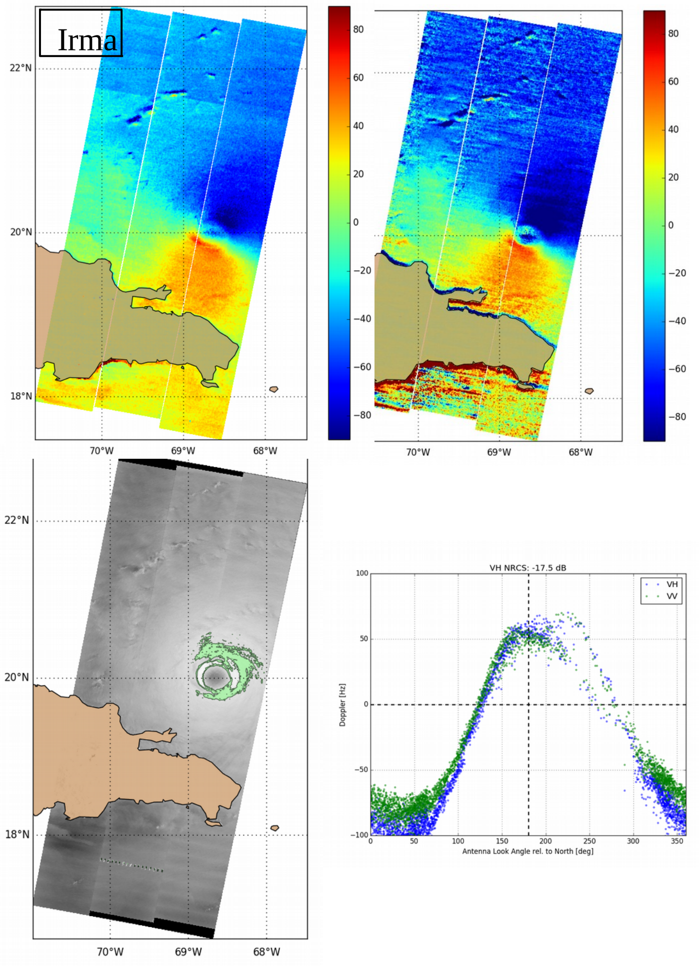

Wave Doppler (bias)

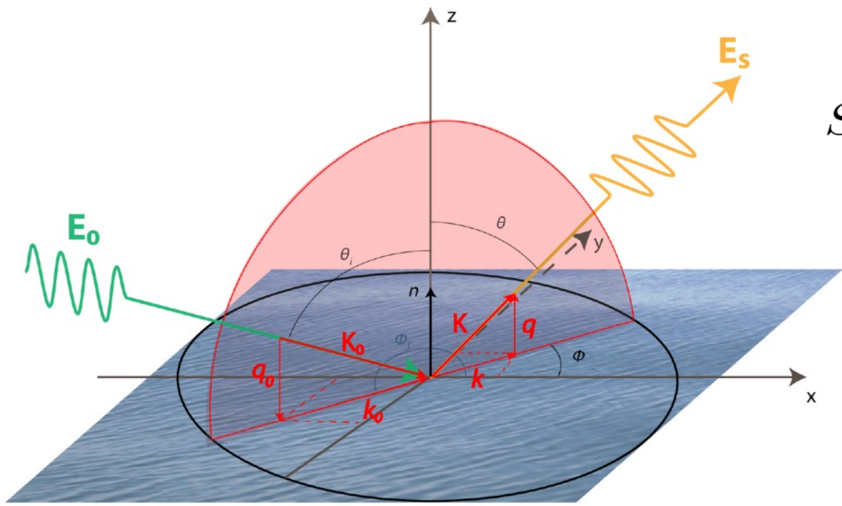

Figure 5: Diffraction (S. Guimbard)

$$S_{KA}(t) \propto \frac{\mathcal{K} \mathrm{e}^{\mathrm{i}K(R-ct)}}{Q_z (2\pi)^2} \int_A d\boldsymbol{r}\ \mathrm{e}^{\mathrm{i}\boldsymbol{Q_H}\cdot\boldsymbol{r}}\ \mathrm{e}^{\mathrm{i}Q_z \eta(\boldsymbol{r},t)}$$

$$\boldsymbol{Q_H} = \boldsymbol{k} - \boldsymbol{k_0}$$
$$Q_z = q + q_0$$

✓ **Sea-state Doppler frequency**

$$f_{\mathrm{GD}} = \frac{Q_z}{2\pi}\left(\mathrm{mss}_{\mathrm{xt}} \frac{\partial_{\tan\theta}\,\psi^0}{\psi^0} + \frac{\mathrm{mss}_{\mathrm{yt}}}{\tan\theta}\frac{\partial_{\varphi}\,\psi^0}{\psi^0}\right)$$

Mean range slope-velocity cross-correlation
NRCS incidence rate of variation
Mean azimuth slope-velocity cross-correlation
NRCS azimuthal rate of variation

A quick focus on the equations

- ✓ **Sigma0 modulations (basic RAR concept equation):**

$$\widetilde{\sigma}^0(x) = \sigma^0 \left(1 + \overline{\partial_x \eta_l}(x) \frac{\partial_{\tan\theta}\sigma^0}{\sigma^0}\right)$$

Range resolved
- wave slopes
- wave velocity

- ✓ **Doppler (velocity) modulations (basic Doppler equation):**

$$2\pi \widetilde{f_{GD}}(x) = Q_z \overline{\partial_t \eta_l}(x) + \frac{Q_z mss_{xt}}{\widetilde{\sigma}^0(x)} \left[\partial_{\tan\theta}\sigma^0 + \overline{\partial_x\eta_l}(x) \frac{\partial^2_{\tan^2\theta}\sigma^0}{\sigma^0}\right]$$

- ✓ **Weighted Doppler modulations :**

$$2\pi \frac{\widetilde{\sigma}^0(x)\widetilde{f_{GD}}(x)}{\sigma^0} = Q_z \overline{\partial_t\eta_l}(x) + Q_z mss_{xt}\overline{\partial_x\eta_l}(x)\frac{\partial^2_{\tan^2\theta}\sigma^0}{\sigma^0} + \dots$$

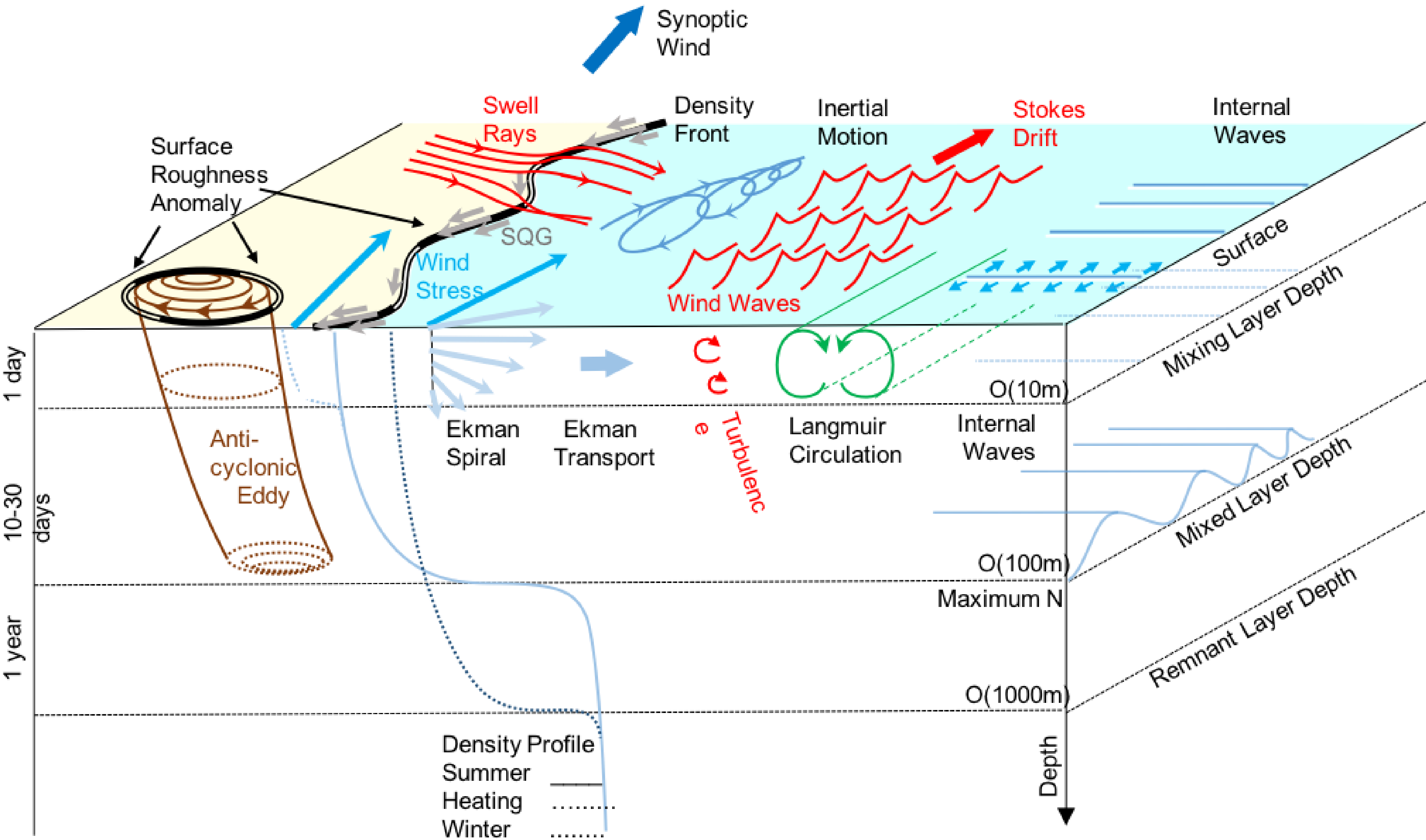
Synoptic Wind
Swell Rays
Density Front
Inertial Motion
Stokes Drift
Internal Waves
Surface Roughness Anomaly
SQG
Wind Stress
Wind Waves
Surface
Mixing Layer Depth
1 day
O(10m)
Ekman Spiral
Ekman Transport
Turbulence
Langmuir Circulation
Internal Waves
Anti-cyclonic Eddy
10-30 days
Mixed Layer Depth
O(100m)
Maximum N
1 year
Remnant Layer Depth
O(1000m)
Density Profile
Summer
Heating
Winter
Depth